DØ note 6027
Version 6

Measurement of the $t\bar{t}$ Production Cross-Section in Dilepton Final State Using RunIIb1 and RunIIb2 Dataset for Winter '10 Conferences

M. Besançon[1], S. Chevalier-Théry[1], A. Croc[1], F. Déliot[1], C. Deterre[1], A. Grohsjean[1], V. Sharyy[1], Y. Peters[2]

[1] Irfu/SPP, CEA-Saclay, France
[2] University of Manchester, UK

(Dated: March 1, 2010)

We present the measurement of the production cross-section for top-antitop events decaying into electron-muon, dimuon or dielectron in proton-antiproton collisions at $\sqrt{s} = 1.96$ TeV using 4.28 fb^{-1} of data collected with the DØ detector from June 2006 to June 2009. The cross-sections after correction for the corresponding expected branching ratios and for a top mass of 172.5 GeV are:

$$\text{ee}: \quad \sigma_{t\bar{t}} = 8.95^{+1.57}_{-1.43}\ (\text{stat})\ ^{+1.39}_{-1.39}\ (\text{syst})\ \pm 0.68\ (\text{lumi})\ \text{pb}$$

$$e\mu: \quad \sigma_{t\bar{t}} = 9.08^{+0.76}_{-0.73}\ (\text{stat})\ ^{+1.01}_{-1.01}\ (\text{syst})\ \pm 0.61\ (\text{lumi})\ \text{pb}$$

$$\mu\mu: \quad \sigma_{t\bar{t}} = 7.24^{+1.46}_{-1.35}\ (\text{stat})\ ^{+1.33}_{-1.43}\ (\text{syst})\ \pm 0.69\ (\text{lumi})\ \text{pb}.$$

The combination of the three channels leads:

$$\ell\ell: \quad \sigma_{t\bar{t}} = 8.76^{+0.61}_{-0.59}\ (\text{stat})\ ^{+1.00}_{-0.95}\ (\text{syst})\ \pm^{+0.67}_{-0.60}\ (\text{lumi})\ \text{pb}$$

Preliminary Results for Winter 2010

Contents

Introduction 3

Data set 3

Event Selection 4
Global Strategy 4
Selection Cuts 4
Optimization of topological selection 6
electron-muon channel 6
dielectron and dimuon channels 7

Event Efficiencies 7

"Fake" Electron Background Evaluation 8
Electron likelihood study with the dielectron sample 9
The background electron likelihood distribution 11
The fake electron background rate calculation 13

"Fake" Muon Background Evaluation 14

Results 16

Systematics 17

Combination 25

Sanity plots 27
Dielectron Channel 27
Electron Muon Channel 36
Dimuon Channel 46

Appendix: TMVA inputs in the dielectron channel 55

Appendix: TMVA inputs in the dimuon channel 56

References 57

I. INTRODUCTION

The analysis presented here is an improved version of 1 fb^{-1} $t\bar{t} \rightarrow e^{\pm}\mu^{\mp}b\bar{b}\nu\bar{\nu}, e^{-}e^{+}b\bar{b}\nu\bar{\nu}, \mu^{-}\mu^{+}b\bar{b}\nu\bar{\nu}$ production cross-section measurements which were published in [1] (analysis DØ notes [2–4]). The previous selections with p20 data are presented in notes [5] for winter 2009 and [6] for summer 2008.

The main differences with published results are:

- Use RunIIb1 and RunIIb2 data set reconstructed with p20 release. These data sets are statistically independent from the previous RunIIa data set (reconstructed with the p17 releases).
- Using *loose* selection for muons instead of *mediumNseg3* and using *loose* selection for tracks matched to muons instead of *medium*.
- Using vertex confirmation for jets (requires that at least 2 tracks from the first primary vertex are associated to jet).
- Final selections have been updated:
  - lower the cut on the H_T variable to 110 GeV (instead of 115 GeV) in the electron-muon final state
  - using a multivariate discriminant in the dielectron final state instead of the topological cut on invariant mass and missing transverse energy
  - using a multivariate discriminant in the dimuon final state instead of the cut on missing transverse energy significance.
- Improve fake muon calculation in electron-muon and dimuon final states: use same-sign events for normalization sample with loose muon isolation cuts ($etHaloScaled < 0.5$ and $etTrkConeScaledMin < 0.5$) instead of no muon isolation at all. The kinematics in this sample are expected to be closer to those of the signal sample.
- Computation of the number of fake electrons separately in the CC and EC calorimeters in the electron-muon and dielectron final states.

All the analysis code is available in the CVS packages *tt_emu_caf, tt_mumu_caf, tt_ee_caf.*

II. DATA SET

The data sample used in this analysis corresponds to all RunIIb1 and RunIIb2 data taken during the period between June 2006 and June 2009. The standard data quality selection was applied to all data [7] (*caf_dq p21-br-03*, *dq_util p21-br-03* and *dq_defs v2009-12-31*). The standard definition from the dq_defs package "dq_defs/common/example.dqdef" has been used. This definition removes bad runs due to the bad SMT, CFT, muon or online calorimeter quality as well as bad luminosity blocks due to the bad offline calorimeter quality. The *DQ* tool also removes events with noise in the calorimeter [8]. The same "bad event quality" removal is applied to the Monte Carlo (MC) samples as a selection and corresponding inefficiencies are taken into account by efficiency calculation. We also remove bad luminosity blocks provided by the luminosity tools. The measured luminosity for this data set is found to be 1618 pb^{-1} for v15 global trigger list and 2662 pb^{-1} for v16 global trigger list. For the electron-muon final state, as for the p17 analysis, to maximize the trigger efficiency, we are using all available triggers (no explicit trigger selection is applied). The efficiency of the "OR" of $e\mu$, single electron and single muon triggers has been measured in Ref. [9] to be more than $\sim$ 95% for v15 for a loose muon selection. We have reevaluated the trigger uncertainty on p20 (see section VIII). For dielectron final state we use an "OR" of the single electron triggers with an efficiency close to 100% [10, 11]. For dimuon final state we use an "OR" of the single muon triggers with an efficiency of about 78% for $t\bar{t} \rightarrow \mu\mu$. Further discussions about the trigger efficiency can be found in the corresponding systematics section (section VIII).

MC samples used in this analysis were generated with the p20.09.03 release. Only requests from the CSG MC definitions are used (*http://www-d0.fnal.gov/Run2Physics/cs/MC/MC.html*). The root CAF trees were produced with the release p21.11.00. All samples are normalized to the NLO theoretical cross-section (or NNLO for Z samples) as implemented in the recent version of caf_mc_util package [13]. Absolute cross-sections used to normalize different invariant mass bins for $Z \rightarrow \ell\ell$ MC samples are calculated as Pythia "leading log" (LL) cross-section for CTEQ6.1 PDF set multiplied by a NNLO/LL(Pythia) K-factors. These K-factors are calculated with the code from Van-Neerman and MRST PDF set (see [14] for some details). For $W \rightarrow \ell\nu$ decays we assume lepton universality and a branching ratio of 0.1080 ± 0.0009 [15]. The cross sections used for the normalization are listed in Table 1 and correspond to the Alpgen cross-section multiplied by the scale factors. As the Z boson p_T is not properly described

in Alpgen, we reweighted the Z p_T distribution for different jet bins. The standard Z p_T reweighting implemented in *caf_mc_util p21-br-143* is used.

Process	Generator	Cross-section used for normalization
$t\bar{t} \to \ell\ell$, $m_t = 172.5\ GeV$	Alpgen+Pythia	7.45 pb
$Z \to \ell\ell$, $m_{\ell\ell} = 15 - 75\ GeV$	Alpgen+Pythia	498 pb
$Z \to \ell\ell$, $m_{\ell\ell} = 75 - 130\ GeV$	Alpgen+Pythia	238 pb
$Z \to \ell\ell$, $m_{\ell\ell} = 130 - 250\ GeV$	Alpgen+Pythia	1.83 pb
$Z \to \ell\ell$, $m_{\ell\ell} > 250\ GeV$	Alpgen+Pythia	0.154 pb
WW inclusive	Pythia	11.6 pb
WZ inclusive	Pythia	3.25 pb
ZZ inclusive	Pythia	1.33 pb

TABLE 1: MC samples used in the analysis with corresponding cross-sections. Lepton ℓ refers here to any lepton: e , μ or τ where τ leptons are decaying inclusively.

The diboson samples are generated by Pythia [34] with the leading order (LO) parton density function CTEQ6L1. The dibosons samples are normalised to the next-to-leading order (NLO) cross section which is about 40 % higher than the LO calculation as performed with the package MCFM. Half of this scale factor is assigned as systematic error on the normalization of the diboson background processes.

III. EVENT SELECTION

1. Global Strategy

The largest background in the dilepton channels comes from $Z \to \ell\ell$ and WW processes with either two electrons, two muons and one electron and one muon in their final states. Other physical backgrounds come from WZ and ZZ processes. These physical backgrounds are evaluated from MC (see section II).

All sources of fake electron background which mainly has a poor electron likelihood [33] are evaluated using a fit on the electron likelihood distribution (see [2] and section V). With this strategy, the QCD background with one fake electron and one fake isolated muon in the electron-muon channel, the $W \to \mu\nu$ background with one fake electron as well as the background processes with γ faking electrons are all computed at the same time. The background contribution coming from fake isolated muons is computed by multiplying the number of events with a loose isolated muons by the muon isolation fake rate (see section VI).

2. Selection Cuts

The general object selection used in the three channels is the following:

1. *Top_tight* electrons are used in electron-muon and dielectron final states. They are defined as follow:
   (a) Electron $|ID|$=10 or 11.
   (b) $|\eta_{calo}| < 2.5$ and exclusion of the ICD region ($|\eta_{calo}| < 1.1$ *or* $|\eta_{calo}| > 1.5$).
   (c) High energy fraction in the EM part of the calorimeter: $f_{EM} > 0.9$.
   (d) Isolated EM cluster: $f_{iso} < 0.15$.
   (e) Shower shape cut: $\chi^2_{hmx7} < 50$.
   (f) $p_T > 15$ GeV (for MC, this corresponds to the smeared electron p_T according to the data / MC difference in energy resolution).
   (g) One track matched with E/p requiring $p_{\chi^2_{\text{trk EOP}}} > 0$ and track $p_T > 5$ GeV.
   (h) Electron likelihood $\mathcal{L}_e > 0.85$.
   (i) Distance between the electron track and the primary vertex: $|z_{electron} - z_{PV}| < 1$ cm.

(j) For MC events, the electron selection efficiency is corrected for the *Top_tight* electron data / MC efficiency difference using standard EM ID correction factors [24]. We are using scale factors dependent on the electron detector η and ϕ.

2. Following muon selection is used for electron-muon and dimuon final states:

   (a) Muon quality definition is *Loose v2*.

      i. *Loose* muon quality.

      ii. $|\eta_{det}| < 2$.

      iii. Timing cuts against cosmic muons background .

   (b) Muon is required to match to a central track with *loose v2* quality.

      i. Quality criteria on the matched track: $|DCA| < 0.04$ cm for tracks with SMT hits and $|DCA| < 0.2$ cm for tracks without SMT hits.

   (c) Distance between the muon track and the primary vertex: $|z_{muon} - z_{PV}| < 1$ cm

   (d) $p_T > 15$ GeV (for MC, this corresponds to the smeared muon p_T according to the data / MC difference in muon momentum resolution).

   (e) Muon isolation is *TopScaledMedium*.

      i. Calorimeter isolation divided by the muon p_T is: $etHaloScaled < 0.15$.

      ii. Tracker isolation divided by the muon p_T is: $etTrkConeScaledMin < 0.15$.

   (f) For MC events, the muon selection efficiency is corrected for the *Loose* muon as well as for the *loose* track and *TopScaledMedium* data / MC efficiency differences using standard muon ID correction factors [26]. We are using scale factors parametrized with the muon ϕ and detector η for the muon quality part and parametrized with z and CFT η and luminosity for the track part and parametrized with CFT η, distance from the jets, muon p_T and luminosity for the isolation part.

3. Jets for all three final states are selected as follows:

   (a) Correct jet p_T with jet energy scale (JES) including muon corrections. Muons identified with the criteria 2 are excluded from the list of muons used for JES correction.

   (b) For simulated jets, the following corrections are applied:

      i. Jet p_T is smeared using SSR procedure.

      ii. Jet with JES corrected $p_T < 15$ GeV are removed (no muon correction applied to JES for this cut).

      iii. SSR "shifting" correction applied to all MC samples except $t\bar{t}$ one.

      iv. Jet reconstruction "plateau" efficiency correction using the jet ID group procedure [27].

   (c) Jet p_T are greater than 20 GeV.

   (d) The absolute value of the jet detector η is less than 2.5.

   (e) EM jet fraction f_{EM} is below 0.95 and above a minimum f_{EM} depending on η_{det} as described in [28].

   (f) The jet coarse hadronic fraction is below an η_{det} dependent cut optimized to reject fake coarse hadronic energy clustered with small random seeds from the inner layers [28].

   (g) The reconstructed jet must be confirmed by the L1 trigger readout.

   (h) The $dR = \sqrt{d\eta_{det}^2 + d\phi^2}$ between the jet and the selected electron is larger than 0.5. If not the jet is rejected.

   (i) Vertex conformation is applied to all jets, which consists in requiring at least two tracks coming from the primary vertex to be present in the jet.

Given the above standard object selections, the list of cuts used to select signal events depending on the dilepton channel considered is the following:

1. Luminosity block selection i.e. removal of "bad" LBN.

2. The calorimeter event quality variables described in the note [8] were required to be good both in data and MC samples. In MC this selection is taken into account in the efficiency calculation and no correction due to this cut is applied.

3. Luminosity [36] and vertex reweightings [18].
4. Vertex selection:
   (a) $|z_{PV}| < 60$ cm.
   (b) Number of tracks associated with the primary vertex greater or equal to 3.
5. Exactly one (electron-muon channel) or two or more (dielectron channel) electrons identified as above.
6. No electrons identified with a selection above are allowed in dimuon channels.
7. One or more (electron-muon channel) or exactly two (dimuon channel) loose muons identified as above.
8. In the electron-muon channel: remove events with $dR(e, \mu) < 0.3$ between electron and muon tracks. This selection significantly suppresses the bremsstrahlung background (a photon emission by the muon, where photon takes the same track as the muon).
9. Choose the two leptons to have opposite charges. If more than one lepton pair is found, choose the lepton pair for which the p_T scalar sum is maximum.
10. Trigger selection in the dielectron and dimuon channels:
    (a) Data sample:
        i. Global trigger selection (single electron or single muon "OR")
        ii. The offline muon, electron and tracks are asked to be matched with the corresponding L1, L2 and L3 objects to be consistent with the trigger efficiency calculation in data.
    (b) For MC, events are weighted according to the calculated trigger efficiency measured in data [10–12] using caf_trigger package.
11. At least 2 jets satisfying the standard selection above are required.
12. Final topological selection:
    (a) In the electron-muon channel, $H_T > 110$ GeV where $H_T = p_T(leading\ lepton) + p_T(2\ leading\ jets)$, where "jets" mean jets satisfying selection criteria above (see Figure 31).
    (b) In the dielectron and dimuon channels, cuts on on the Boosted Decision Tree outputs are applied. This Boosted Decision Trees are trained to separate the $t\bar{t}$ process from the Z/γ^* and diboson background processes. The optimization of this final topological selection is described in section III 3.

3. Optimization of topological selection

electron-muon channel

In order to find the optimal final topological cut, we have used the following figure of merit based on MC prediction for signal and background: $FM = \frac{\sqrt{S+B}}{S}$ where S is the number of estimated $t\bar{t} \to e\mu$ events with a luminosity of 4.28 fb^{-1} and B is the number of diboson and $Z \to \tau\tau$ background events after the 2 jet selection. As in the previous version of the analysis [1, 2], we have studied the cuts on two parameters: the missing transverse energy and the H_T variable. Varying the cuts on those two parameters, the best set of cuts will be found when the figure of merit is minimum. The result of the optimization is shown in Figure 1. Adding the number of fake events in the computation of FM doesn't change significantly the optimal point. We then choose a cut at $H_T > 110$ GeV and no MET cut as optimal final topological cut.

It has to be noticed that multivariate techniques have been also tried to look if a better optimal point can be found. But due to the low number of MC events remaining after the 2 jet selection, it was not possible to correctly train any of these multivariate discriminants. In addition due to the high purity that has been already achieved in the electron-muon channel, this was not expected to significantly further improve the final selection.

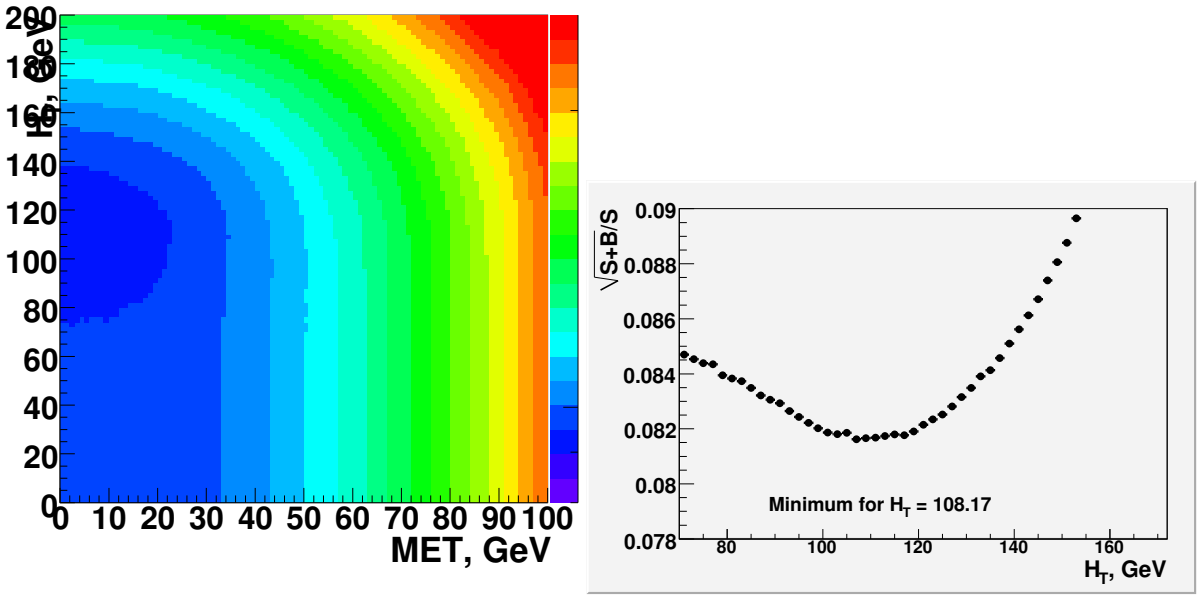

FIG. 1: Variation of $\sqrt{S+B}/S$ as a function of the H_T and MET cuts (left) and H_T cut (right).

dielectron and dimuon channels

In order to improve the purity in the same flavor dilepton channels, Boosted Decision Trees have been used. For that purpose, the MC samples have been divided in two equal parts: one part for the training of the BDT inside TMVA [19] and one part for the event yield determination. For the training, $t\bar{t} \to ee$ or $\mu\mu$ MC events are used for the signal and $Z/\gamma^* \to ee$ or $\mu\mu$ and diboson MC events are used for the background. The same variables as in the W helicity analysis [20] are used as inputs to the BDTs: aplanarity, centrality, sphericity (see definitions in [20]), H_T, the sum of the jets and leptons energies: H, MET, MET significance [23], the minimum distance in the $\eta - \phi$ space between the closest pair of jets multiplied by the E_T of the lowest E_T jet in the pair, and divided by the E_T of the W ($k't_{min}$), the minimum dijet mass of all jet pairs (M_{jjmin}), and the dilepton invariant mass ($M_{\ell\ell}$). The aplanarity, centrality, sphericity are computed using the jets and the selected leptons. The data/MC agreement for these variables can be found in sections X A and X C. The signal/background variable separations and the correlations between the variables are shown in Appendix XI and XII.

We use 500 trees boosted using "AdaBoost". "gini" is used as cut ranking algorithm. A maximum of 50 cuts is set. Pruning is also used with the "CostComplexity" method [19]. It has to be noticed that even if the current used BDTs give good results, further optimizations on the BDTs parameters may still be possible. The BDT ouputs for the training and testing samples in the dielectron and dimuon channels are shown in Figure 2.

The data/MC BDT discriminants before cut are shown in Figure 3.

To find what would be the optimal cut on the BDT outputs, we computed the same figure of merit based on MC prediction for signal and background as in the electron-muon channel: $FM = \frac{\sqrt{S+B}}{S}$ where S is the number of estimated $t\bar{t} \to ee$ or $\mu\mu$ events with a luminosity of 4.28 fb^{-1} and B is the number of diboson and Z/γ^* background events. The variation of this figure of merit with the cut on the BDT outputs can be found in Figure 4.

We can see that FM for both channels shows a rather flat minimum. A parabolic fit has been used to find optimal values: $BDT_{ee} > 0.51$ and $BDT_{\mu\mu} > 0.5$. This selection improves by more than 5% the value of FM obtained in previous version of the selection using simple cuts.

IV. $t\bar{t}$ EVENT EFFICIENCIES

For the signal MC, we are using $t\bar{t} \to ll$ events generated by Alpgen+Pythia [34, 37] using leading order (LO) parton density function CTEQ6L1. The efficiencies of the selection are shown for different generated top quark masses for the different dilepton channels in Table 2.

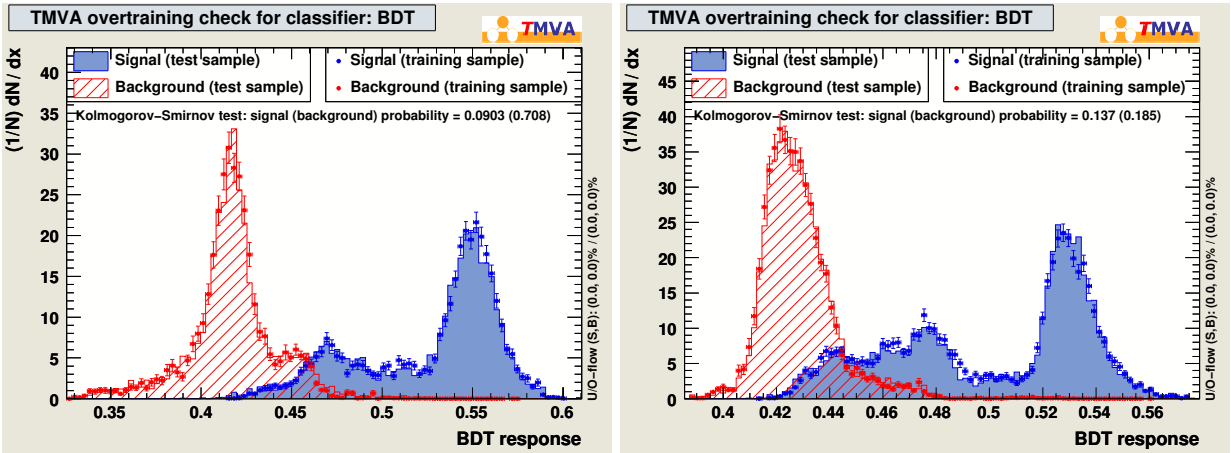

FIG. 2: Dielectron (left) and dimuon (right) BDT ouputs for the signal (blue) and background (red) samples using the training samples (histograms) and the testing samples (points).

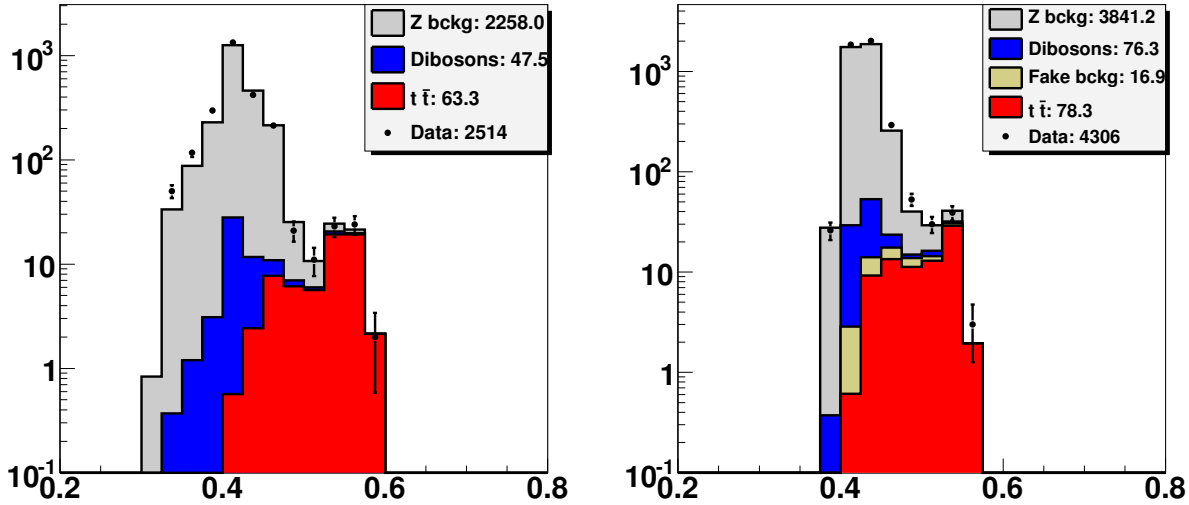

FIG. 3: Data/MC BDT output distribution before cut in the dielectron channel (left) and dimuon channel (right).

V. "FAKE" ELECTRON BACKGROUND EVALUATION

This section describes the method for evaluating the "fake" electron background that is identical to the one in [2]. "Fake electron" refers to a jet misidentified as an electron as well as to real electrons produced by jets, e.g. in the case of b quark semileptonic decay. These second types of "fake electrons" indeed are real electrons. Mostly these electrons are not isolated and tend to have a low likelihood value. In the following we will continue to use the expression "fake electron" for both types of events. This background is mainly composed of multijet events (QCD) including light or heavy flavor jets. It may also contain $W \to \mu\nu_\mu$, $t\bar{t} \to \mu jjjj$ and $\mu \to \mu\gamma$ processes.

In order to separate the background from the signal, we use the 8-variable electron likelihood distribution [33]. The likelihood distribution for the signal has a peak around 1 and the background distribution peaks mainly near 0 (see for example Figure 5 and 6). Using the shape of the electron likelihood distribution measured with a sample of real electrons and the shape for "fake electrons" measured in a sample dominated by multijet background, one can fit the electron likelihood distribution for the selected events to determine the number of signal and background events separately in the CC and EC.

The study of the electron likelihood in a dielectron sample is discussed in subsection V A below. We then discuss the fit procedure and the shape of the electron likelihood. We check the p_T dependence as well as the number of

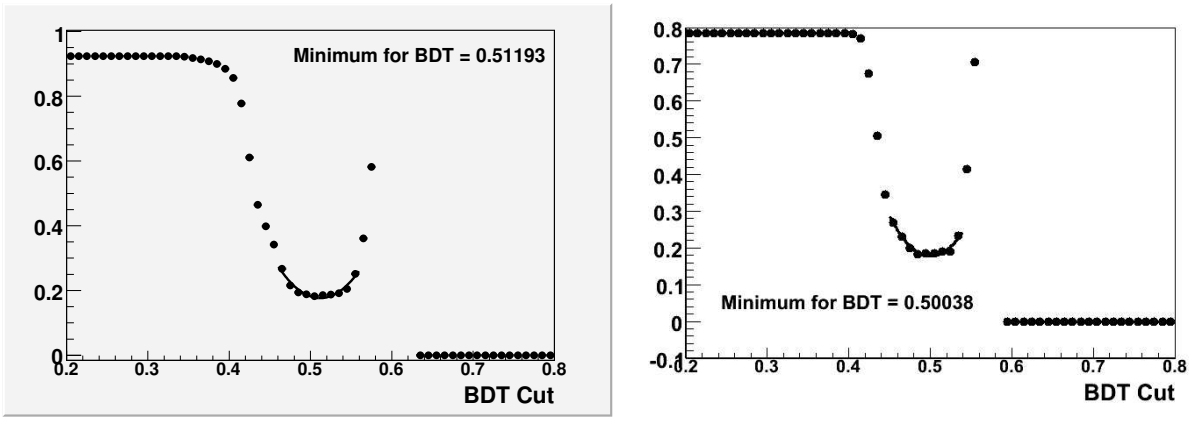

FIG. 4: Variation of $\sqrt{S+B}/S$ as a function of the dielectron BDT cut (left) and dimuon BDT cut (right).

TABLE 2: Selection efficiencies for $t\bar{t} \to ee$, $t\bar{t} \to e\mu$ and $t\bar{t} \to \mu\mu$ for different generated top quark masses. The $t\bar{t}$ efficiency is calculated relative to the inclusive $t\bar{t} \to ll$ final state after the final selection. This includes all the electron, muon and τ decays of the W from the top's. The quoted errors are statistical only.

Top quark Mass	$t\bar{t} \to ee$ Efficiency	$t\bar{t} \to e\mu$ Efficiency	$t\bar{t} \to \mu\mu$ Efficiency
130 GeV	$0.58 \pm 0.01\%$	2.19 ± 0.02 %	0.76 ± 0.01 %
135 GeV	$0.65 \pm 0.01\%$	2.52 ± 0.02 %	0.82 ± 0.01 %
140 GeV	$0.71 \pm 0.01\%$	2.77 ± 0.03 %	0.91 ± 0.01 %
150 GeV	$0.84 \pm 0.01\%$	3.42 ± 0.03 %	1.09 ± 0.01 %
160 GeV	$0.96 \pm 0.01\%$	3.87 ± 0.01 %	1.21 ± 0.01 %
165 GeV	$1.03 \pm 0.01\%$	4.07 ± 0.02 %	1.25 ± 0.01 %
170 GeV	$1.07 \pm 0.01\%$	4.25 ± 0.02 %	1.33 ± 0.01 %
172.5 GeV	$1.10 \pm 0.01\%$	4.27 ± 0.02 %	1.36 ± 0.01 %
175 GeV	$1.12 \pm 0.01\%$	4.40 ± 0.01 %	1.37 ± 0.01 %
180 GeV	$1.17 \pm 0.01\%$	4.57 ± 0.02 %	1.44 ± 0.01 %
185 GeV	$1.22 \pm 0.01\%$	4.68 ± 0.02 %	1.49 ± 0.01 %
190 GeV	$1.26 \pm 0.01\%$	4.85 ± 0.02 %	1.55 ± 0.01 %
195 GeV	$1.32 \pm 0.01\%$	4.92 ± 0.03 %	1.56 ± 0.02 %
200 GeV	$1.34 \pm 0.02\%$	5.10 ± 0.04 %	1.62 ± 0.02 %
205 GeV	$1.36 \pm 0.02\%$	5.09 ± 0.04 %	1.62 ± 0.02 %
210 GeV	$1.41 \pm 0.02\%$	5.24 ± 0.04 %	1.72 ± 0.02 %

jet dependence of the electron likelihood shape. The study of the background shape is described in subsection V B. Finally, the procedure for computing the fake electron background rate is discussed in subsection V C which closes this section.

A. Electron likelihood study with the dielectron sample

In order to study the electron likelihood shape, a dielectron data sample is used. The selection criteria require 2 loose electrons with opposite charges selected with *top_tight* criteria, dropping the likelihood cut on one randomly chosen electron from the two (i.e. that corresponds to one *top_loose* electron and one *top_tight* electron). Dropping the likelihood requirement on a randomly chosen electron allows to remove any potential bias on the likelihood shape due to the electron p_T for instance. The missing transverse energy corrected with jet energy scale and muon p_T is less than 15 GeV. The invariant dielectron mass is required to be in the range 70 – 110 GeV.

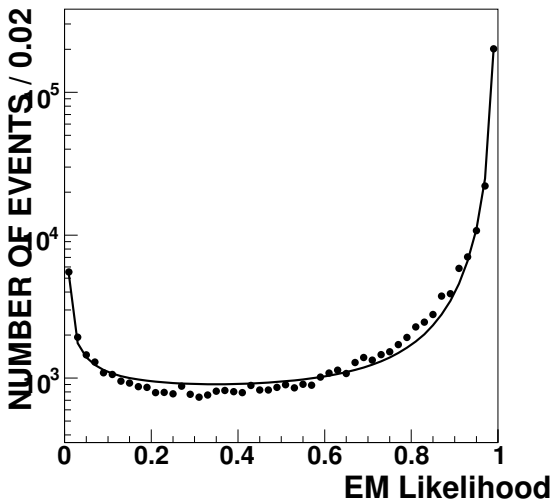

(a) Inclusive sample (no jet requirement) in CC

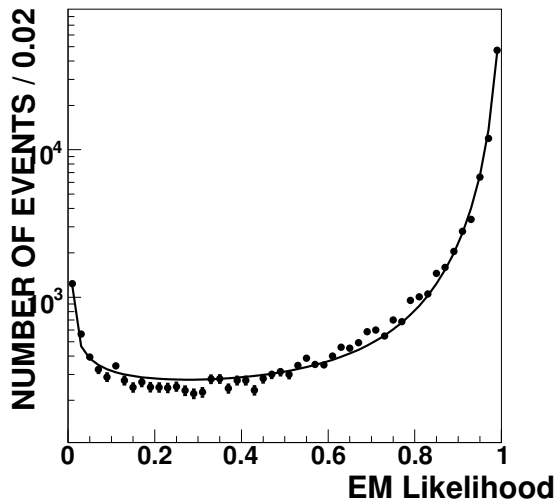

(b) Inclusive sample (no jet requirement) in EC

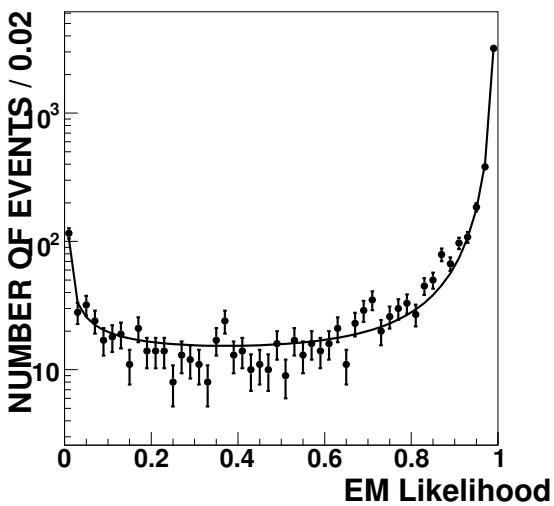

(c) 2 jet inclusive in CC

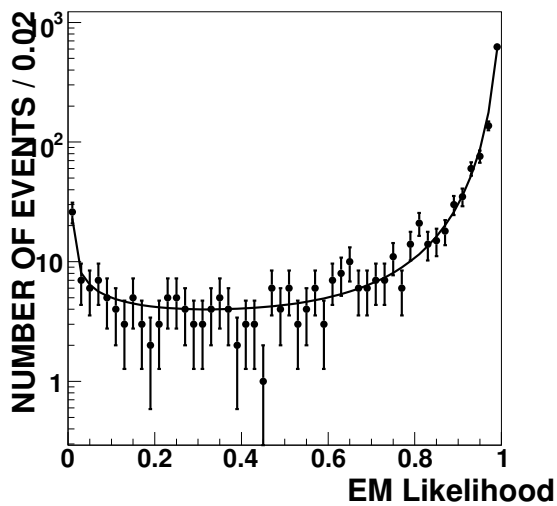

(d) 2 jet inclusive in EC

FIG. 5: The electron likelihood distributions for electrons from $Z \to ee$ in data. The solid line represents the fit function. The function value drawn in the bin center corresponds to the fit function integral for the bin.

a. Fit procedure

In order to fit the distribution, an extended unbinned likelihood method is used [38]. The likelihood is written as:

$$\mathscr{L} = \frac{e^{-n}}{N!} \prod_{i=1}^{N} nP(x_i, c_0, c_1, \alpha_0, \alpha_1, \mu_0, \mu_1), \tag{1}$$

where i is an event number, N is the total number of observed events, n is a free parameter in the fit, P is a probability distribution function (p.d.f.) normalized to 1 (eq. 2), x_i is the electron likelihood for event i, $c_0, c_1, \alpha_0, \alpha_1, \mu_0, \mu_1$ are

the p.d.f. parameters (free parameters in the fit). It was found that the following p.d.f. gives a good description:

$$P = c_0 \frac{(\alpha_0 - 1)(\mu_0 - x_i)^{-\alpha_0}}{(\mu_0 - 1)^{1-\alpha_0} - \mu_0^{1-\alpha_0}} + c_1 \frac{(1 - \alpha_1)(\mu_1 + x_i)^{-\alpha_1}}{(\mu_1 + 1)^{1-\alpha_1} - \mu_1^{1-\alpha_1}} + c_2, \text{ with } c_0 + c_1 + c_2 = 1 \tag{2}$$

here the parameter μ_0 is slightly greater than 1, and μ_1 is close, but greater than 0. In order to find the parameters, the whole dielectron selection is applied to the sample. The likelihood of the loose electron is used in the fit to find the optimal set of parameters to describe the electron likelihood distribution depending if it is in the CC or EC. Table 3 and Figure 5 shows the fit results after the 2 jet selection. The c_0 parameter represents the fraction of events peaked at a likelihood value near 1, c_1 is the fraction of events peaked near 0 and c_2 is the uniformly distributed events. The parameters α_0, μ_0 and α_1, μ_1 are highly correlated and describe the form of the distribution.

TABLE 3: Electron likelihood p.d.f. parameters, found with the unbinned extended likelihood method for the dielectron sample for the 2 jet selection. The sum $c_0 + c_1 + c_2$ is normalized to 1.

	c_0	μ_0	α_0	c_1	μ_1	α_1	c_2
CC	$0.845^{+0.013}_{-0.014}$	$1.003^{+0.000}_{-0.000}$	$1.720^{+0.006}_{-0.006}$	$0.056^{+0.005}_{-0.005}$	$6.5^{+1.5}_{-1.2} \cdot 10^{-5}$	$0.771^{+0.014}_{-0.014}$	$0.099^{+0.008}_{-0.008}$
EC	$0.855^{+0.028}_{-0.028}$	$1.016^{+0.000}_{-0.000}$	$1.967^{+0.019}_{-0.019}$	$0.064^{+0.014}_{-0.013}$	$1.0^{+0.0}_{-0.0} \cdot 10^{-7}$	$0.652^{+0.013}_{-0.013}$	$0.080^{+0.019}_{-0.018}$

b. *Electron p_T dependence*

In order to measure the electron likelihood distribution dependence on the electron p_T, the loose electrons were divided into several subsamples according to their p_T. The fit procedure is repeated independently for each subsample. The shape of the distribution itself, characterized by the parameters $\alpha_0, \alpha_1, \mu_0, \mu_1$ does not show any dependence with p_T (the parameters α and μ agree within statistical errors). A p_T dependence can be seen for the parameters c_0, c_1, c_2 which characterizes the relative fraction of events with "good" and "non-isolated" electrons. So in the following, the parameters $\alpha_0, \alpha_1, \mu_0, \mu_1$ are fixed at their values from Table 3 and only parameters c_0, c_1, c_2 were fitted. The obtained results are shown in Tables 4 and 5. One can see a clear p_T dependence. This can be most probably understood by the fact that high p_T electrons have a lower probability to be matched to a wrong track because of the bigger difference between the electron energy and the randomly chosen track momentum.

TABLE 4: The electron likelihood fit dependence on electron p_T for CC electrons (dielectron sample)

p_T limits	c_0	c_1	c_2
15 GeV $< p_T <$ 25	$0.792^{+0.012}_{-0.012}$	$0.093^{+0.006}_{-0.006}$	$0.114^{+0.008}_{-0.008}$
25 GeV $< p_T <$ 35	$0.845^{+0.006}_{-0.006}$	$0.057^{+0.003}_{-0.003}$	$0.099^{+0.004}_{-0.004}$
35 GeV $< p_T <$ 45	$0.871^{+0.004}_{-0.004}$	$0.034^{+0.001}_{-0.001}$	$0.095^{+0.002}_{-0.002}$
45 GeV $< p_T <$ 55	$0.892^{+0.007}_{-0.007}$	$0.025^{+0.002}_{-0.002}$	$0.083^{+0.003}_{-0.003}$
55 GeV $< p_T <$ 65	$0.905^{+0.049}_{-0.048}$	$0.020^{+0.013}_{-0.010}$	$0.075^{+0.023}_{-0.022}$
65 GeV $< p_T <$ 75	$0.933^{+0.157}_{-0.141}$	$0.000^{+0.040}_{-0.000}$	$0.067^{+0.060}_{-0.051}$
75 GeV $< p_T$	$0.912^{+0.128}_{-0.117}$	$0.013^{+0.047}_{-0.000}$	$0.075^{+0.069}_{-0.060}$

c. *Dependence on the number of jet*

Z events with jets have higher detector occupancy than Z events without jets, and hence higher probability for electrons to be matched to a wrong track. The dependence on the number of jets for the likelihood distribution is shown in Table 6 (here again the parameters $\alpha_0, \alpha_1, \mu_0, \mu_1$ are fixed at their values from Table 3). We use the parameters obtained with 2 jet events for the electron likelihood function in the $t\bar{t} \to e\mu$ 2 jet inclusive selection.

B. The background electron likelihood distribution

In order to find the background distribution, a background dominated sample with the same topology as the signal has been selected. We are using the electron-muon selection for that purpose. The standard electron-muon

TABLE 5: The electron likelihood fit dependence on electron p_T for EC electrons (dielectron sample)

p_T limits	c_0	c_1	c_2
15 GeV $< p_T <$ 25	$0.841^{+0.012}_{-0.012}$	$0.069^{+0.006}_{-0.006}$	$0.090^{+0.008}_{-0.008}$
25 GeV $< p_T <$ 35	$0.885^{+0.008}_{-0.008}$	$0.028^{+0.003}_{-0.003}$	$0.087^{+0.005}_{-0.005}$
35 GeV $< p_T <$ 45	$0.883^{+0.007}_{-0.007}$	$0.025^{+0.003}_{-0.003}$	$0.092^{+0.004}_{-0.004}$
45 GeV $< p_T <$ 55	$0.896^{+0.018}_{-0.017}$	$0.040^{+0.007}_{-0.007}$	$0.064^{+0.011}_{-0.010}$
55 GeV $< p_T <$ 65	$0.786^{+0.124}_{-0.113}$	$0.000^{+0.033}_{-0.000}$	$0.214^{+0.077}_{-0.065}$
65 GeV $< p_T <$ 75	$0.495^{+0.679}_{-0.349}$	$0.505^{+0.685}_{-0.353}$	$0.000^{+0.258}_{-0.000}$
75 GeV $< p_T$	$0.509^{+0.731}_{-0.377}$	$0.000^{+0.533}_{-0.000}$	$0.491^{+0.718}_{-0.443}$

TABLE 6: The dependence of the electron likelihood distribution shape with the number of jets for CC electrons (dielectron sample).

	c_0	c_1	c_2
CC 0 jet	$0.857^{+0.002}_{-0.002}$	$0.044^{+0.001}_{-0.001}$	$0.099^{+0.002}_{-0.002}$
CC 1 jet	$0.849^{+0.005}_{-0.005}$	$0.049^{+0.001}_{-0.001}$	$0.101^{+0.003}_{-0.003}$
CC 2 jets	$0.845^{+0.014}_{-0.013}$	$0.056^{+0.005}_{-0.005}$	$0.099^{+0.008}_{-0.008}$
EC 0 jet	$0.876^{+0.004}_{-0.004}$	$0.040^{+0.002}_{-0.002}$	$0.083^{+0.004}_{-0.004}$
EC 1 jet	$0.860^{+0.010}_{-0.010}$	$0.051^{+0.004}_{-0.004}$	$0.089^{+0.007}_{-0.006}$
EC 2 jets	$0.855^{+0.028}_{-0.028}$	$0.064^{+0.013}_{-0.013}$	$0.080^{+0.019}_{-0.018}$

selection criteria were applied except for the muon isolation. In order to remove the physics background contamination from $Z \to \tau\tau$ and diboson, events with anti-isolated muons were selected with $etHaloScaled > 0.15$ and $etTrkConeScaled > 0.15$ and the missing transverse energy had to be less than 15 GeV. The background electron likelihood distribution are shown for the inclusive and 2 jets samples in Figure 6 and the parameters are summarized in Tables 7 and 8. Tables 9 and 10 show the variation of the parameters with the electron p_T which will be used to assign systematic error on the fake electron background determination.

TABLE 7: Fake electron likelihood p.d.f. parameters, found with the unbinned extended likelihood method (2 jet requirement). The sum $c_0 + c_1 + c_2$ is normalized to 1.

	c_0	μ_0	α_0	c_1	μ_1	α_1	c_2
CC	$0.160^{+0.028}_{-0.026}$	$1.006^{+0.006}_{-0.006}$	$0.927^{+0.244}_{-0.119}$	$0.819^{+0.045}_{-0.044}$	$2.6^{+0.4}_{-0.4} \cdot 10^{-5}$	$1.054^{+0.000}_{-0.014}$	$0.021^{+0.033}_{-0.000}$
EC	$0.175^{+0.040}_{-0.037}$	$1.033^{+0.062}_{-0.021}$	$1.249^{+0.787}_{-0.363}$	$0.801^{+0.064}_{-0.061}$	$2.6^{+0.1}_{-0.8} \cdot 10^{-5}$	$0.946^{+0.025}_{-0.022}$	$0.024^{+0.054}_{-0.000}$

TABLE 8: Fake electron likelihood p.d.f. parameters, found with the unbinned extended likelihood method. The sum $c_0+c_1+c_2$ is normalized to 1.

	c_0	c_1	c_2
CC 0 jet excl	$0.101^{+0.016}_{-0.019}$	$0.899^{+0.038}_{-0.039}$	$0.000^{+0.026}_{0.000}$
CC 1 jet excl	$0.102^{+0.012}_{-0.012}$	$0.898^{+0.030}_{-0.029}$	$0.000^{+0.013}_{0.000}$
CC 2 jet incl	$0.160^{+0.028}_{-0.026}$	$0.819^{+0.045}_{-0.044}$	$0.021^{+0.003}_{0.000}$
EC 0 jet excl	$0.110^{+0.036}_{-0.032}$	$0.871^{+0.074}_{-0.071}$	$0.018^{+0.057}_{0.000}$
EC 1 jet excl	$0.093^{+0.017}_{-0.016}$	$0.907^{+0.040}_{-0.039}$	$0.000^{+0.014}_{0.000}$
EC 2 jet incl	$0.175^{+0.040}_{-0.037}$	$0.801^{+0.064}_{-0.061}$	$0.024^{+0.054}_{0.000}$

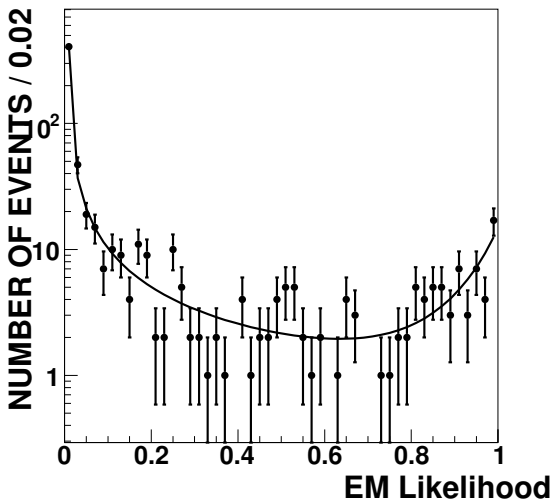

(a) Inclusive sample (no jet requirement) in CC

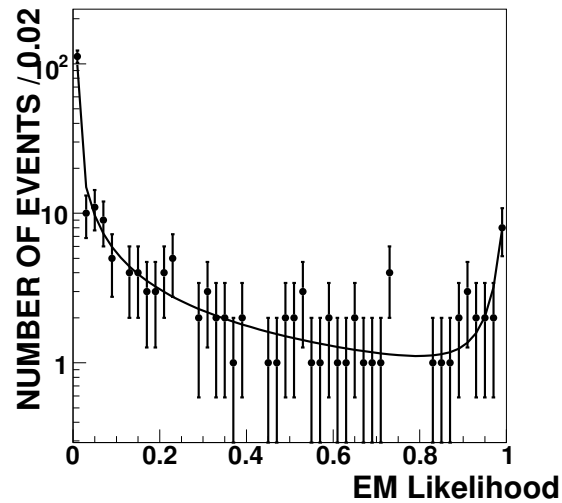

(b) Inclusive sample (no jet requirement) in EC

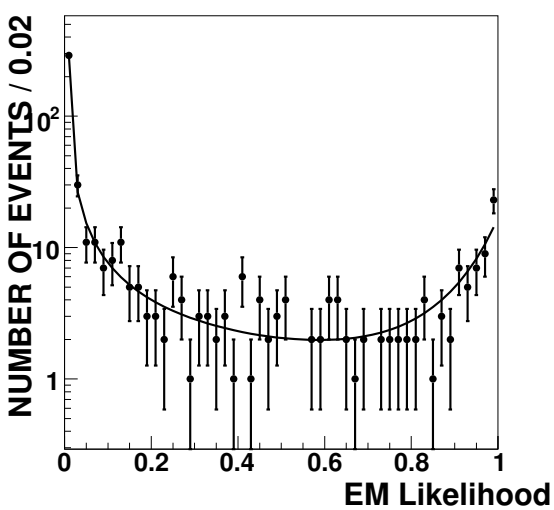

(c) 2 jet inclusive selection in CC

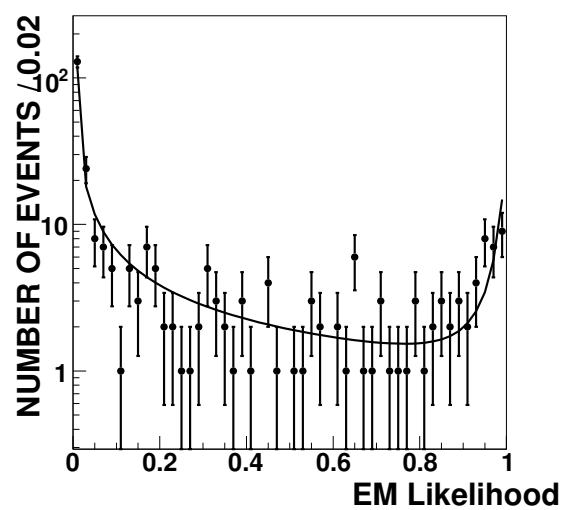

(d) 2 jet inclusive selection in EC

FIG. 6: The electron likelihood distributions for the background sample. The solid line represents the fit function. The function value drawn in the bin center corresponds to the fit function integral for the bin.

C. The fake electron background rate calculation

In order to calculate the number of events with fake and isolated electrons, an unbinned likelihood fit is used with the following likelihood:

$$\mathscr{L} = \frac{e^{-(n_e+n_{fake})}}{N!}\prod_{i=1}^{N}(n_e S(x_i) + n_{fake}B(x_i)), \tag{3}$$

where i is the event number, x_i is the electron likelihood value, N is the total number of selected events, n_e is the number of events with an isolated electron, n_{fake} is the number of events with a fake electron. S is the signal probability distribution function (p.d.f.) normalized to 1 described by function (2) where μ_0, α_0, μ_1 and α_1 are fixed

TABLE 9: The electron likelihood fit dependence on electron p_T for CC electrons (fake electron sample)

p_T limits	c_0	c_1	c_2
15 GeV $< p_T <$ 25	$0.133^{+0.019}_{-0.018}$	$0.853^{+0.033}_{-0.032}$	$0.014^{+0.023}_{-0.000}$
25 GeV $< p_T <$ 35	$0.103^{+0.017}_{-0.015}$	$0.897^{+0.040}_{-0.039}$	$0.000^{+0.014}_{-0.000}$
35 GeV $< p_T <$ 45	$0.075^{+0.021}_{-0.019}$	$0.925^{+0.056}_{-0.054}$	$0.000^{+0.019}_{-0.000}$
45 GeV $< p_T <$ 55	$0.090^{+0.031}_{-0.026}$	$0.910^{+0.077}_{-0.073}$	$0.000^{+0.028}_{-0.000}$
55 GeV $< p_T <$ 65	$0.163^{+0.075}_{-0.073}$	$0.820^{+0.124}_{-0.113}$	$0.017^{+0.095}_{-0.000}$
65 GeV $< p_T <$ 75	$0.189^{+0.076}_{-0.062}$	$0.811^{+0.138}_{-0.124}$	$0.000^{+0.032}_{-0.000}$
75 GeV $< p_T$	$0.298^{+0.081}_{-0.070}$	$0.702^{+0.115}_{-0.104}$	$0.000^{+0.063}_{-0.000}$

TABLE 10: The electron likelihood fit dependence on electron p_T for EC electrons (fake electron sample)

p_T limits	c_0	c_1	c_2
15 GeV $< p_T <$ 25	$0.139^{+0.038}_{-0.034}$	$0.745^{+0.061}_{-0.058}$	$0.115^{+0.056}_{-0.054}$
25 GeV $< p_T <$ 35	$0.155^{+0.037}_{-0.034}$	$0.798^{+0.060}_{-0.057}$	$0.048^{+0.050}_{-0.000}$
35 GeV $< p_T <$ 45	$0.072^{+0.030}_{-0.032}$	$0.928^{+0.074}_{-0.079}$	$0.000^{+0.059}_{-0.000}$
45 GeV $< p_T <$ 55	$0.059^{+0.032}_{-0.026}$	$0.941^{+0.086}_{-0.081}$	$0.000^{+0.015}_{-0.000}$
55 GeV $< p_T <$ 65	$0.046^{+0.039}_{-0.030}$	$0.954^{+0.112}_{-0.104}$	$0.000^{+0.029}_{-0.000}$
65 GeV $< p_T <$ 75	$0.072^{+0.056}_{-0.039}$	$0.928^{+0.153}_{-0.138}$	$0.000^{+0.023}_{-0.000}$
75 GeV $< p_T$	$0.041^{+0.042}_{-0.028}$	$0.959^{+0.135}_{-0.124}$	$0.000^{+0.022}_{-0.000}$

to the values found in Table 3 and c_0, c_1 and c_2 are taken from Table 6 depending on the number of jets required. B is the background probability distribution function (p.d.f.) normalized to 1 described by function (2) where μ_0, α_0, μ_1 and α_1 are fixed to the values found in Table 7 and c_0, c_1 and c_2 are taken from Table 8 depending on the number of jets required.

The number of fake electrons in the electron-muon channel is then extracted after fitting the likelihood of the electron before the likelihood cut. The number of fake electrons in the dielectron channel is extracted in the same way when requiring randomly one tight and one loose electrons. The likelihood distributions in the final samples are shown in Figure 7 for the ee channel and in Figure 8 for the $e\mu$ channel.

As a cross check to this evaluation we can look at the number of same sign (SS) dilepton events after the final selection. In the $e\mu$ channel, we found a good agreement between the number of fake electron and muon estimation with the number of SS events (~ 10 events while we evaluate the sum of the fake electron and fake muon background to be: $10.7^{+4.1}_{-3.9}$, see Table 13). In the dielectron channel, we have 4 SS events after the final selection from which we should substract the contribution from the misidentification of electron charge (~ 1 event) and SS diboson contribution (not estimated). Our fake electron background estimation in this channel is: $0.1^{+0.2}_{-0.1}$ (see Table 12).

VI. "FAKE" MUON BACKGROUND EVALUATION

This type of background comes from events with at least one fake isolated muon coming mainly from heavy flavor quark decays. In the electron-muon channel, it comes more precisely from events with one fake isolated muon and one isolated electron ($W \to e\nu$, $Z \to ee$ and $t\bar{t} \to ejjj$). Because the fake muon isolation rate is low especially when requiring two jets, this background is low. In order to estimate this background, we first estimate the fake muon rate in data using $b\bar{b}$ events and then estimate the number of fake muon background using a same sign selection with a loose isolation requirement in our signal sample.

To measure the muon isolation fake rate f_μ i.e. the rate at which a muon appears isolated in events where it should not, we select dimuon loose events matched to loose tracks with one non isolated matched muon as a tag ($etHaloScaled > 0.15$, $etTrkConeScaledMin > 0.15$, near a jet : $dR(\mu, jet) < 0.5$) with $p_T > 15$ GeV and count the number of muons with $p_T > 15$ GeV that appear isolated as a probe. We estimated this rate as a function of the number of extra jets. Figure 9 shows this fake rate for the 2 jet selection as a function of MET. As some signal contamination from W events with large MET can be seen, we used only the low MET region ($MET < 40$) to compute the fake rate. The results are shown in Table 11.

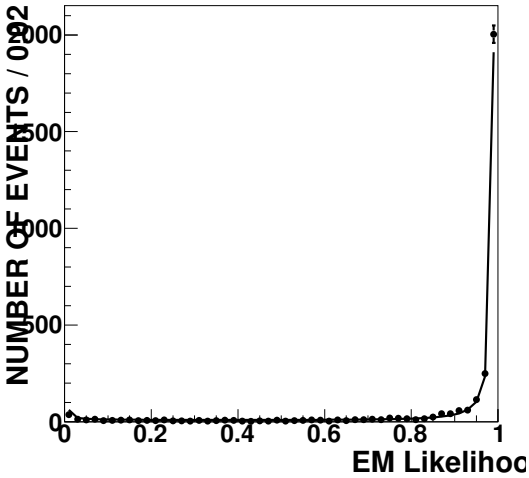

(a) 2 jet inclusive selection in CC

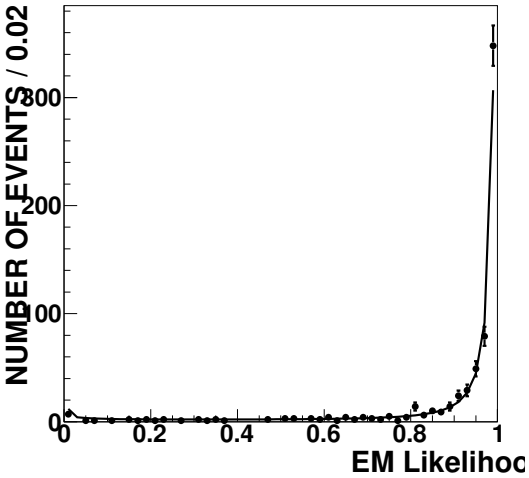

(b) 2 jet inclusive selection in EC

FIG. 7: The electron likelihood distributions for the final sample in the ee channel. The solid line represents the fit function. The function value drawn in the bin center corresponds to the fit function integral for the bin.

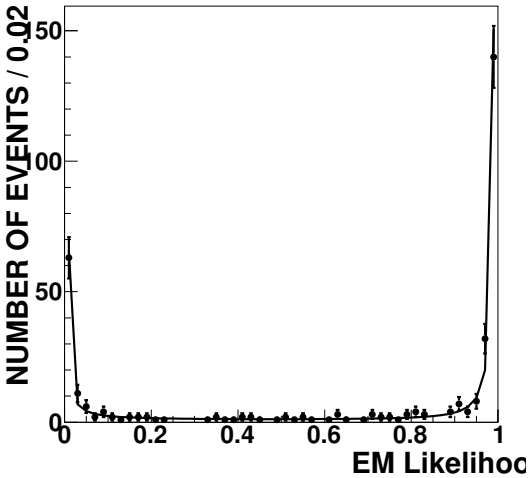

(a) 2 jet inclusive selection in CC

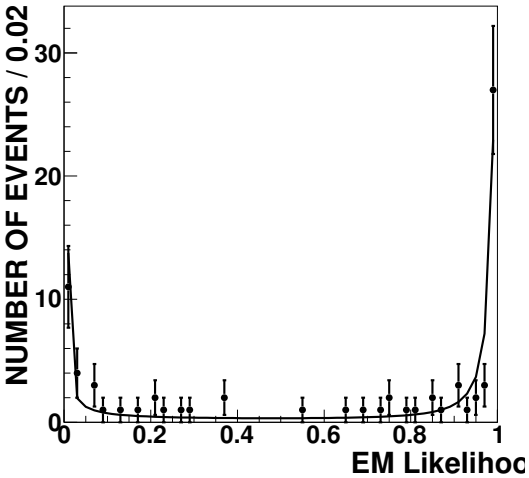

(b) 2 jet inclusive selection in EC

FIG. 8: The electron likelihood distributions for the final sample in the $e\mu$ channel. The solid line represents the fit function. The function value drawn in the bin center corresponds to the fit function integral for the bin.

TABLE 11: Fake muon isolation rate for different number of jet requirement (the errors quoted are statistical only).

	0 jet exclusive	1 jet exclusive	2 jets inclusive
f_μ	34.88 ± 1.02 %	16.15 ± 0.74 %	16.10 ± 1.17 %

To compute the number of fake muon background events in our signal sample we then start from the data sample in the electron-muon or dimuon channels and apply the same selection as for the signal (1-12) except that we don't require any isolation for the muons but we ask for the two selected leptons to have the same charge to prevent

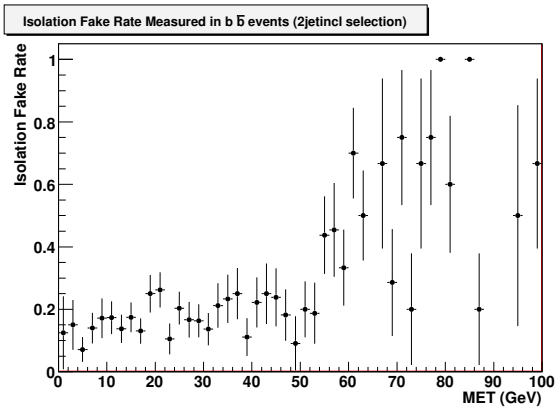

FIG. 9: Muon isolation fake rate as a function of MET after the 2 jet selection.

contamination from physics background. We also subtract the estimated contribution from fake electron background using the likelihood fit technique in the electron-muon channel.

The number of events in our selection coming from fake muon isolation background is then estimated as the number of events in the "same sign loose isolation" selection times the fake muon isolation rate computed above. In the dimuon channel, the "same sign loose isolation" sample is obtained by loosening the isolation requirement on only one muon. In the electron-muon channel the number of same charge events with loose muon isolation requirement after fake electron substraction is: 20 events (for CC) and 1.6 evts (for EC) after final selection except likelihood cut. Taking into account the efficiency of the likelihood cut determined from the fit (see section V) and multiplying by the fake muon rate from Table 11, we obtain $2.6^{+1.1}_{-0.9}$ (see Table 13).

VII. RESULTS

The number of events expected for the different MC samples and observed in data are presented in Table 12 for the dielectron channel, in Table 13 for the electron-muon channel and in Table 14 for the dimuon channel.

TABLE 12: The measured and predicted event yield in $t\bar{t} \to ee$ process. The errors shown include all systematic uncertainties (except the one from the luminosity).

	$Z \to \ell\ell$	Dibosons	Number of fake electron events	$tt \to \ell\ell jj$, xsec=7.454 pb, m_t =172GeV)	Expected N of events	N of events
Inclusive selection	$161255.9^{+21667.0}_{-21668.1}$	$262.2^{+56.2}_{-56.2}$	$0.0^{+0.3}_{-0.0}$	$77.7^{+7.1}_{-7.2}$	$161595.8^{+21680.7}_{-21681.9}$	155459
N jets ≥ 1	$19385.9^{+4397.4}_{-4391.2}$	$111.1^{+25.3}_{-25.3}$	$0.0^{+0.3}_{-0.0}$	$75.3^{+7.0}_{-7.0}$	$19572.4^{+4408.8}_{-4402.5}$	19433
N jets ≥ 2	$2258.0^{+875.9}_{-866.6}$	$47.5^{+11.8}_{-11.8}$	$0.0^{+0.2}_{-0.0}$	$52.7^{+5.5}_{-5.5}$	$2358.2^{+883.2}_{-873.9}$	2514
MV Selection: BDT $\geq$ 0.51	$8.5^{+3.4}_{-3.4}$	$2.1^{+0.8}_{-0.8}$	$0.1^{+0.2}_{-0.1}$	$36.9^{+3.8}_{-3.8}$	$47.6^{+6.2}_{-6.2}$	55

The number of $t\bar{t}$ events is obtained after subtraction of the MC predictions for the "physics" backgrounds (WW, WZ and Z/γ^*) and of the "fake" electron and muon contributions. The statistical errors on the cross-section are determined by extended likelihood fit of the resulting number of events using Poisson distribution. The likelihood function used in this fit is the following:

$$\mathscr{L} = (\sigma_{t\bar{t}}\varepsilon_{t\bar{t}}L_{int} + n_{bckg})^N \frac{e^{-(\sigma_{t\bar{t}}\varepsilon_{t\bar{t}}L_{int}+n_{bckg})}}{N!}, \tag{4}$$

where N is the observed number of events, n_{bckg} is the expected number of background events, $\varepsilon_{t\bar{t}}$ is the $t\bar{t}$ efficiency, L_{int} is the integrated luminosity and $\sigma_{t\bar{t}}$ is the fitted $t\bar{t}$ cross-section.

Using the efficiencies from Table 2, the integrated luminosity of 4.28 fb^{-1} and the $t\bar{t} \to \ell\ell$ branching ratio of 0.10498 the $p\bar{p} \to t\bar{t}$ cross-section is found to be:

TABLE 13: The measured and predicted event yield in $t\bar{t} \to e\mu$ process. The errors shown include all systematic uncertainties (except the one from the luminosity).

	$Z \to \tau\tau$	Dibosons	Number of fake electron events	Number of fake muon events	$tt \to \ell\ell jj$, xsec=7.454 pb, m_t =172GeV)	Expected N of events	N of events
Inclusive selection	$2085.2^{+298.2}_{-265.1}$	$350.7^{+74.1}_{-74.1}$	$220.5^{+99.9}_{-99.9}$	-	$210.6^{+17.8}_{-17.8}$	$2866.9^{+341.3}_{-312.7}$	2975
N jets ≥ 1	$289.2^{+63.9}_{-58.7}$	$55.6^{+14.8}_{-14.5}$	$74.8^{+35.3}_{-35.3}$	$11.4^{+2.4}_{-2.3}$	$205.2^{+17.4}_{-17.4}$	$636.3^{+86.8}_{-82.4}$	684
N jets ≥ 2	$28.2^{+13.9}_{-12.5}$	$9.2^{+2.7}_{-2.7}$	$15.0^{+7.0}_{-6.9}$	$1.8^{+1.2}_{-1.1}$	$147.9^{+14.6}_{-14.6}$	$202.2^{+24.2}_{-23.1}$	234
HT (with leading lepton) $\geq$ 110 GeV	$11.9^{+2.7}_{-2.5}$	$6.5^{+2.1}_{-2.0}$	$8.1^{+3.9}_{-3.8}$	$2.6^{+1.1}_{-0.9}$	$143.4^{+14.3}_{-14.3}$	$172.6^{+16.5}_{-16.4}$	204

TABLE 14: The measured and predicted event yield in $t\bar{t} \to \mu\mu$ process. The errors shown include all systematic uncertainties (except the one from the luminosity).

	$Z \to \ell\ell$	Dibosons	Number of fake muon events	$tt \to \ell\ell jj$, xsec=7.454 pb, m_t =172GeV)	Expected N of events	N of events
Inclusive selection	$258522.0^{+34728.0}_{-35710.3}$	$381.0^{+80.1}_{-80.1}$	-	$109.5^{+8.9}_{-8.9}$	$259012.4^{+34745.0}_{-35727.0}$	238633
N jets ≥ 1	$34358.5^{+8333.6}_{-7962.2}$	$170.6^{+37.1}_{-36.9}$	$52.2^{+3.8}_{-3.7}$	$106.9^{+8.7}_{-8.7}$	$34688.2^{+8346.3}_{-7974.5}$	31443
N jets ≥ 2	$3841.2^{+1646.9}_{-1570.0}$	$76.3^{+18.3}_{-18.3}$	$16.9^{+2.1}_{-2.0}$	$80.6^{+7.7}_{-7.7}$	$4015.1^{+1657.0}_{-1580.2}$	4306
MV Selection: BDT $\geq$ 0.5	$21.7^{+5.6}_{-6.2}$	$3.3^{+1.1}_{-1.2}$	$3.2^{+0.8}_{-0.7}$	$45.1^{+4.4}_{-4.3}$	$73.3^{+8.1}_{-8.8}$	72

$$\text{ee}: \quad \sigma_{t\bar{t}} = 8.95^{+1.57}_{-1.43}\,(\text{stat})\,^{+1.39}_{-1.39}\,(\text{syst})\ \pm 0.68\,(\text{lumi})\,\text{pb}$$

$$e\mu: \quad \sigma_{t\bar{t}} = 9.08^{+0.76}_{-0.73}\,(\text{stat})\,^{+1.01}_{-1.01}\,(\text{syst})\ \pm 0.61\,(\text{lumi})\,\text{pb}$$

$$\mu\mu: \quad \sigma_{t\bar{t}} = 7.24^{+1.46}_{-1.35}\,(\text{stat})\,^{+1.33}_{-1.43}\,(\text{syst})\ \pm 0.69\,(\text{lumi})\,\text{pb}.$$

The estimation of the systematic uncertainties is described in the following section.

VIII. SYSTEMATICS

Here the systematic uncertainties related to our measurements are discussed.

- **Luminosity uncertainty**. The luminosity uncertainty is known to be 6.1% [50]. To obtain the luminosity error on the cross section we apply this uncertainty both on MC $t\bar{t}$ signal samples and on the background evaluated from MC in a correlated way.

- **Systematics due to Data-MC luminosity profile difference**. The DØ simulation uses overlaid zero bias events to reproduce detector and luminosity effects from real data. This requires an exact matching of the overlaid zero bias luminosity profile to the luminosity profile in data. In order to reduce the impact of this discrepancy on the selection, the luminosity reweighting procedure has been used in MC [36]. This procedure increases the weights of MC events with high luminosity. Unfortunately, the exact match of luminosity profile requires very high weights for MC events with high luminosity. In order to limit the statistical fluctuation because of the high individual weight, the maximal allowed weight in the luminosity reweighting procedure has been set to 3. In order to estimate the systematics due to the imperfection of the matching procedure all MC samples have been reweighted without any maximal limit on the weight and the difference in the efficiency with the default case (maximal weight equals to 3). This uncertainty is found to be negligible (less than 0.1%).

- **Systematics due to the MC statistics**. This systematic error originates from the statistical error on the selection efficiencies.

- **Systematics due to the $W \to l$ branching ratio error**. This systematic error is computed by propagating the error on the W to lepton branching ratio assuming lepton universality [15].

- **Data quality flag systematics**. The systematic uncertainty on the measured data quality flag efficiency was estimated to be 0.5% [17].

- **Higher order effects and hadronization**. This uncertainty is evaluated by comparing Alpgen+Pythia with MC@NLO. For more details see [51]. As currently the size of the MC samples used to evaluate these uncertainties are limited, we are quoting the maximum between the statistical error and the difference between Alpgen+Pythia and MC@NLO as systematic uncertainty. This uncertainty has been evaluated in the electron-muon channel and ported in the dielectron and dimuon channels.

- **Color reconnection systematics**. This uncertainty is evaluated by comparing Pythia tune Apro with Pythia tune ACRpro. For more details see [51]. As currently the size of the MC samples used to evaluate these uncertainties are limited, we are quoting the maximum between the statistical error and the difference between Pythia tune Apro with Pythia tune ACRpro as systematic uncertainty. This uncertainty has been evaluated in the electron-muon channel and ported in the dielectron and dimuon channels.

- **ISR/FSR systematics**. This uncertainty is evaluated by comparing Pythia with the varied ISR/FSR parameters. The range of variation has been determined by CDF. For more details see [51]. As currently the size of the MC samples used to evaluate these uncertainties are limited, we are quoting the maximum between the statistical error and the difference between the different between the different MC samples. This uncertainty has been evaluated in the electron-muon channel and ported in the dielectron and dimuon channels.

- **PDF uncertainties**. The standard *caf_pdfreweight* package has been used for this estimation. The systematic uncertainty due to the choice of PDF is estimated by varying the 20 CTEQ6.1M PDF within their errors in the $t\bar{t}$ signal MC [44]. As our MC samples are generated using CTEQ6.1L, we have to consider the reweight efficiency from CTEQ6.1L to CTEQ6.1M as central value for this uncertainty determination.

- **b-quark fragmentation uncertainty**. This error is estimated using the standard procedure described in [45] by reweighting the $t\bar{t}$ events using different fragmentation functions.

- **Muon ID and track scale factor systematics**. We use as the uncertainties on loose muons and loose tracks the numbers provided by the muon ID group [26].

- **Muon isolation scale factor systematics**. We use as the uncertainties on the muon isolation the number provided by the muon ID group [26].

- **Trigger systematics**. In the dielectron channel, the evaluation of the systematic uncertainties on the single electron "OR" trigger efficiency is done in two steps. We first evaluate the influence of the statistical uncertainties on the trigger turn-ons by shifting them by $\pm\sigma$. The difference between data and MC changes by +0.3% -0.5%. We then select only one random electron before applying the trigger turn-on. If the trigger turn-ons didn't have any uncertainties, the difference between MC and data should stay the same. This difference shifts by 0.7%, which is of the order of the variation induced by the statistical uncertainties. We then quote the statistical uncertainties on the turn ons as electron trigger systematic uncertainty.

  In dimuon channel we apply similar technique. The statistical uncertainty on the trigger efficiency is found to be 5%. After selecting one random muon we found that the difference between data and MC is changed less than statistical uncertainty and we assign 5% as trigger systematicsin dimuon channel.

  In electron-muon channel we compare data and MC after applying the single electron "OR" trigger requirement or the single muon "OR" requirement. The data/MC ratio changes by 5.3% for single electron "OR" and by 7% for the single muon "OR". We choose to use the single electron trigger "OR" result to assign the systematics, as this trigger OR is more efficient and known to be better measured than single muon "OR"

- **Opposite charge requirement systematics**. The electron charge misidentification fraction is not the same in data and in MC. To evaluate the systematic uncertainty on the opposite sign requirement, we had to evaluate these fractions, both for MC and data, in the CC and the EC. We used the $Z \to ee$ MC samples, and required successively opposite and same sign events. We fitted the invariant mass distributions to keep only events in the Z peak, and computed the misID fraction for one electron in the EC and the CC. They are presented in Table 15.

	Data	MC
CC	0.24	0.06
EC	5.8	2.7

TABLE 15: Electron charge misidentification fraction (in %)

The obtained results are consistent with those of the EMID group [43]. We then computed the probability to have same sign events in the background and signal samples in MC and data. We assign the difference of these probabilities as the systematic uncertainty on the opposite sign requirement. We have studied this misidentification fraction in $Z \to \mu\mu$ events and found it negligeable.

- **Uncertainty from the dZ cut**. Our selection requires that the distance along the beam axis between the lepton tracks and the vertex is less than 1 cm. It has been found recently that the efficiency of this cut can be very different between MC and data. To measure it we have computed the MC/data ratio of this distance prior to any cuts as a function of the jet multiplicity. After requiring 2 jets, we have found an efficiency difference of 2% for this cut between data and MC (both in dimuon and dielectron final state) that we assigned as systematic uncertainty.

- **Z vertex distribution difference between data and MC**. The z vertex distribution simulated in MC events is quite different from the data. In order to correct for this difference the corresponding p20 reweighting from the *caf_mc_util* package has been applied. This reweighting is based on the study from the note [18]. In order to estimate the systematics for this correction, an alternative parametrization for the beam shape could be used. The difference in the event selection efficiency between default and alternative parametrization is quoted as a systematic uncertainty.

- **Electron ID scale factor systematics**. The uncertainties on the Electron ID scale factor have been determined by the EMID group [47] taking into account the fluctuations in the data and MC efficiencies used to obtain the scale factor and the background contributions in the certification procedure. The default parametrization of the electron identification efficiency is two-dimensional and uses detector η and ϕ. Other parametrizations exist with respect to p_T, luminosity and the vertex position. Using all the different parametrizations, we noticed that the biggest difference in efficiency comes from changing the parameterization from (η, ϕ) to (η, p_T). In addition to the error coming from the certification procedure, we assign these differences as systematic uncertainties for the electron identification efficiency.

- **Electron smearing systematics**. In standard analyses, additional smearing is applied to MC electrons to take into account the difference of resolution between data and MC. This oversmearing is currently being improved by the EMID group. For the moment we use a 0.5% uncertainty on the current used parameters to evaluate the systematic uncertainty due to the electron resolution [48]. This uncertainty is found to be negligible.

- **Lepton momentum scale systematics**. This systematic uncertainty emerges from the electron and muon momentum scale difference between data and simulation. It is evaluated by varying the electron and muon momentum scale as described in [51].

- **Muon resolution systematics**. In standard analyses, additional smearing is applied to MC muon to take into account the difference of resolution between data and MC. The systematic uncertainty due to this additionnal smearing is evaluated by shifting the smearing parameters by their uncertainties [49].

- **Jet ID systematics**. The standard procedure defined by the jet ID group has been used which consists of varying the jet ID efficiency by its uncertainty.

- **Jet resolution systematics**. The JSSR procedure applies additional smearing to the MC jets, in order to account for the different jet p_T resolution in data and MC. To compute the systematic uncertainty on the jet resolution, the width of the gaussian used to smear the jet energy should be varied by the size of the uncertainty on the jet energy resolution parameters in MC.

- **Vertex confirmation systematics**. The uncertainty on the jet vertex confirmation efficiency is evaluated by the jet ID group and implement in the caf_eff_util package. We estimated this uncertainty by varying the vertex confirmation efficiency scale factor by one standard deviation.

- **Jet energy scale systematics**. This systematic error has been evaluated by shifting the JES corrections by -1σ or $+1\sigma$ where σ has been measured in the JSSR procedure [31].

- **b-quark JES**. This error takes into account the difference between the nominal inclusive JES and the JES for b-hadrons. This later JES has been evaluated to be 1.8 % smaller [46]. This systematic error is obtained by shifting down by 1.8 % the nominal JES.

- **JSSR shifting systematics**. As the JSSR jet shifting has been derived on γ+jets and Z+jets events and so is not fully valid for the MC samples used in the analysis due to the different fraction of gluon and quark jets in the samples, a systematic error has been conservatively assigned by switching off the shifting correction for the background samples and by switching on the shifting correction for $t\bar{t}$. The errors on the background and on the signal are taken to be uncorrelated.

- **Uncertainties on diboson and $Z \to \ell\ell$ cross-sections.** These uncertainties have been discussed in section II.

- **Z p_T reweighting uncertainty.** In this analysis, we use the new Alpgen Z pT reweighting (*caf_mc_util* p21-br-143), which computes two weights (inclusive and per bin of jets) and their systematic uncertainties. Shifting these weights by their positive and negative uncertainties induces a difference in the Z efficiency. We quote this efficiency changes as systematic error on the Z pT reweighting by conservatively adding the inclusive and jet dependent uncertainties quadratically.

- **Background modeling uncertainty.** To taken into account the disagreement between data and MC BDT shapes in the dielectron or dimuon channels we have reweighted the Z MC samples to the data in a background dominated region ($BDT < 0.5$). We see a difference of 10% in the background yield after reweighting consistent with the largest effect observed when reweighting the input BDT variables. We quote this variation as systematic uncertainty on the background samples.

- **Likelihood fit statistics**. This error comes from the uncertainty of the electron likelihood fit.

- **Likelihood fit systematics for the fake electron background**. The main source of systematic uncertainty from the likelihood fit procedure comes from the uncertainty on the c_0 parameter for the background template that mostly determines the number of fake electron background after likelihood cut (the other ones are correlated to it). The largest variation of this parameter comes from the dependency on the electron p_T. We are using the variations of c_0 seen in Tables 9 and 10 for the background template to determine this systematic error. We assigned a 50% uncertainty on the number of fake electron background in CC and 100% uncertainty on the number of fake electron background in EC.

- **Fake muon systematic uncertainties.** An uncertainty due to the statistical error on the fake muon rate determination and on the statistical error of the non isolated muon sample have been assigned to the fake muon background estimation.

- **Cross-section dependence with the top mass**. The uncertainty due to the effect of the top mass on the full selection efficiency is estimated using MC samples generated with different top masses. Following the general top group strategy, we will not add this systematics to all other sources, but it will be cited separately. This allows to recalculate the cross-section for any value of the top mass.

  Using the same parametrization as in [1], we fit the measured cross section as a function of the top quark mass. The variation of the combined p17 and p20 measurement (cf. eq. 6) as a function of the top mass is shown in Fig 10.

The total systematic errors for the different MC samples are summarized in the tables 16, 17 and 18 including all systematic errors except the error on the top mass. We call the variations of the systematics uncertainties "up", if it shifts the $t\bar{t}$ efficiency to the larger values. Usually it corresponds to the negative shift on the cross-section and hence to to the "down" variation of total cross section.

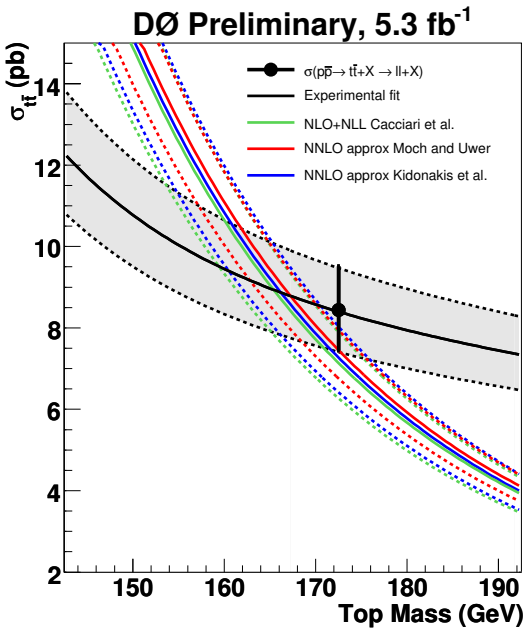

FIG. 10: Variation of the measured cross section (point) as a function of the top quark mass (black lines). Also shown the theoritical prediction (red, green and blue lines) from [39, 52, 53].

TABLE 16: Relative systematics for the different MC samples in the dielectron channel.

	$t\bar{t} \to \ell\ell jj$, %		$Z \to \ell\ell$, %		Dibosons, %		Fake EM, %		Total, pb	
	up	down	up	down	up	down	up	down	down	up
MC statistics	1.11	-1.11	20.03	-20.03	18.59	-18.59			-0.37	0.37
$W \to \ell\nu$ branching ratio	1.70	-1.70							-0.15	0.15
DQ event selection	0.50	-0.50	0.50	-0.50	0.50	-0.50			-0.06	0.06
Higher order and hadronization	2.00	-2.00							-0.18	0.18
Color reconnection	2.60	-2.60							-0.23	0.23
ISR/FSR	3.40	-3.40							-0.30	0.30
PDF	0.54	-0.86	3.76	-4.06	1.66	-1.37			-0.12	0.15
b quark modeling	1.24	-1.24							-0.11	0.11
Trigger	0.50	-0.50	0.50	-0.50	0.50	-0.50			-0.06	0.06
Opposite charge	1.64	-1.64	1.64	-1.64	1.64	-1.64			-0.18	0.18
dZ(lepton, PV)	2.00	-2.00	2.00	-2.00	2.00	-2.00			-0.22	0.22
Electron ID (certification)	6.80	-6.80	6.80	-6.80	6.80	-6.80			-0.75	0.75
Electron ID (p_T dependence)	1.85	-1.85	3.36	-3.36	5.40	-5.40			-0.25	0.25
EM energy scale	0.71	-0.71	-9.92	9.92	6.26	-6.26			0.08	-0.08
Vertex Z distribution	0.24	-0.24	8.66	-8.66	0.84	-0.84			-0.17	0.17
Jet ID	1.11	-1.11	1.07	-1.07	2.35	-2.35			-0.13	0.13
Jet resolution	0.58	-0.58	-5.49	5.49	5.89	-5.89			0.02	-0.02
Vertex confirmation	2.39	-2.39	17.71	-17.71	10.78	-10.78			-0.56	0.56
Jet energy scale	1.81	-1.92	16.21	-16.26	8.69	-8.20			-0.48	0.49
b quark JES	0.44	-0.44							-0.04	0.04
JSSR shifting on	3.37	-3.37							-0.30	0.30
Z cross-section			5.00	-5.00					-0.09	0.09
Z p_T reweighting			10.00	-10.00					-0.17	0.17
Background modeling			10.00	-10.00	10.00	-10.00			-0.21	0.21
JSSR shifting off			11.47	-11.47	12.82	-12.82			-0.25	0.25
Diboson cross-section					20.00	-20.00			-0.09	0.09
Fit statistical error							165.22	-81.40	-0.04	0.02
Fit systematics							50.00	-50.00	-0.01	0.01
Total:	10.38	-10.42	40.22	-40.27	36.97	-36.85	172.62	-95.53	1.39	-1.39

TABLE 17: Relative systematics for the different MC samples in the electron-muon channel.

	$t\bar{t} \to \ell\ell jj$, %		$Z \to \tau\tau$, %		Dibosons, %		Fake EM, %		Fake Mu, %		Total, pb	
	up	down	up	down	up	down	up	down	up	down	down	up
MC statistics	0.43	-0.43	10.79	-10.79	10.91	-10.91					-0.09	0.09
$W \to \ell\nu$ branching ratio	1.70	-1.70									-0.15	0.15
DQ event selection	0.50	-0.50	0.50	-0.50	0.50	-0.50					-0.05	0.05
Higher order and hadronization	2.00	-2.00									-0.18	0.18
Color reconnection	2.60	-2.60									-0.24	0.24
ISR/FSR	3.40	-3.40									-0.31	0.31
PDF	0.28	-0.48	6.15	-4.49	0.53	-0.65					-0.07	0.07
b quark modeling	1.09	-1.09									-0.10	0.10
Muon ID	1.00	-1.00	1.00	-1.00	1.00	-1.00					-0.10	0.10
Muon track	1.10	-1.10	1.10	-1.10	1.10	-1.10					-0.11	0.11
Muon isolation	0.50	-0.50	0.50	-0.50	0.50	-0.50					-0.05	0.05
Trigger	5.00	-5.00	5.00	-5.00	5.00	-5.00					-0.50	0.50
Opposite charge	0.82	-0.82	0.82	-0.82	0.82	-0.82					-0.08	0.08
dZ(lepton, PV)	2.00	-2.00	2.00	-2.00	2.00	-2.00					-0.20	0.20
Electron ID (certification)	3.40	-3.40	3.70	-3.70	3.40	-3.40					-0.34	0.34
Electron ID (p_T dependence)	0.80	-0.80	-0.92	0.92	0.36	-0.36					-0.07	0.07
EM energy scale	0.19	-0.19	2.43	-2.43	0.13	-0.13					-0.03	0.03
Vertex Z distribution	0.55	-0.55	0.59	-0.59	0.39	-0.39					-0.05	0.05
Jet ID	1.01	-1.01	0.75	-0.75	2.52	-2.52					-0.10	0.10
Jet resolution	0.22	-0.15	-0.17	-0.05	2.18	0.09					-0.03	0.01
Vertex confirmation	2.66	-2.66	1.99	-1.99	6.10	-6.10					-0.27	0.27
Jet energy scale	1.52	-1.69	4.31	-3.23	6.54	-5.04					-0.19	0.19
b quark JES	0.72	-0.72									-0.07	0.07
JSSR shifting on	4.09	-4.09									-0.37	0.37
Z cross-section			5.00	-5.00							-0.03	0.03
Z p_T reweighting			9.40	-8.00							-0.06	0.05
JSSR shifting off			12.48	-12.48	18.26	-18.26					-0.14	0.14
Diboson cross-section					20.00	-20.00					-0.07	0.07
Fit statistical error							16.01	-14.39	39.52	-34.91	-0.09	0.08
Fit systematics							45.01	-45.01			-0.19	0.19
Fake muon rate									7.29	-7.29	-0.01	0.01
Total:	9.96	-10.00	22.35	-21.20	31.43	-31.08	47.77	-47.25	40.19	-35.66	1.01	-1.01

TABLE 18: Relative systematics for the different MC samples in the dimuon channel.

	$t\bar{t} \to \ell\ell jj$, %		$Z \to \ell\ell$, %		Dibosons, %		Fake Mu, %		Total, pb	
	up	down	up	down	up	down	up	down	down	up
MC statistics	0.95	-0.95	15.25	-15.25	17.86	-17.86			-0.56	0.56
$W \to \ell\nu$ branching ratio	1.70	-1.70							-0.12	0.12
DQ event selection	0.50	-0.50	0.50	-0.50	0.50	-0.50			-0.06	0.06
Higher order and hadronization	2.00	-2.00							-0.14	0.14
Color reconnection	2.60	-2.60							-0.19	0.19
ISR/FSR	3.40	-3.40							-0.25	0.25
PDF	0.13	-0.25	2.74	-2.71	1.19	-1.07			-0.11	0.12
b quark modeling	0.96	-0.96							-0.07	0.07
Muon ID	2.00	-2.00	2.00	-2.00	2.00	-2.00			-0.23	0.23
Muon track	2.20	-2.20	2.20	-2.20	2.20	-2.20			-0.25	0.25
Muon isolation	1.00	-1.00	1.00	-1.00	1.00	-1.00			-0.11	0.11
Trigger	5.00	-5.00	5.00	-5.00	5.00	-5.00			-0.57	0.57
dZ(lepton, PV)	2.00	-2.00	2.00	-2.00	2.00	-2.00			-0.23	0.23
Vertex Z distribution	0.50	-0.50	1.11	-1.11	0.43	-0.43			-0.08	0.08
Jet ID	0.44	-0.44	-0.23	0.23	2.29	-2.29			-0.04	0.04
Jet resolution	0.25	-0.19	6.12	-14.34	-3.48	-7.33			-0.22	0.57
Vertex confirmation	2.34	-2.34	3.52	-3.52	12.45	-12.45			-0.36	0.36
Jet energy scale	1.96	-1.73	0.33	-1.28	4.49	-13.41			-0.18	0.24
b quark JES	0.86	-0.86							-0.06	0.06
JSSR shifting on	4.06	-4.06							-0.29	0.29
Z cross-section			5.00	-5.00					-0.18	0.18
Z p_T reweighting			8.20	-7.60					-0.29	0.27
Background modeling			10.00	-10.00	10.00	-10.00			-0.41	0.41
JSSR shifting off			11.69	-11.69	-2.45	2.45			-0.41	0.41
Diboson cross-section					20.00	-20.00			-0.11	0.11
Statistical error on SS							24.06	-20.73	-0.13	0.11
Fake muon rate							7.29	-7.29	-0.04	0.04
Total:	9.65	-9.61	25.68	-28.63	32.53	-35.49	25.14	-21.97	1.33	-1.43

IX. COMBINATION

The combination of all dilepton channels is done in the same way as previously [40, 41] by performing a maximum likelihood fit of the predicted number of events, dependent on $\sigma_{t\bar{t}}$, to the observed number of events. In order to take into account each channel into the likelihood maximization procedure the Poisson probabilities are multiplied together:

$$\mathscr{L} = \prod_{i=1} P(N_i^{\rm obs}, N_i^{\rm predicted}(\sigma_{t\bar{t}})) \tag{5}$$

where $P(N_i^{\rm obs}, N_i^{\rm predicted})$ defines the Poisson probability to observe $N^{\rm obs}$ events when the predicted number of events is $N^{\rm predicted}$ and where i runs over all three channels.

The correlation of systematic uncertainties between the channels is taken into account by assigning the same nuisance parameter to each correlated systematic [42]. The correlations between each channel and between p20 and p17 are summarized in Table 19. Each nuisance parameter is varied one at a time by 1 σ up and down, and the difference between the newly determined cross section and the central result denotes the systematic uncertainty for the considered systematics. The total systematic uncertainty is calculated by taking the quadratic sum of all systematics.

TABLE 19: Summary of the systematic uncertainties correlations between each channel in p20 (left) and between p20 and p17 measurements (right).

Systematic	p20 ee	p20 $e\mu$	p20 $\mu\mu$
Correlated			
Branching fractions	X	X	X
Data quality	X	X	X
Higher order, hadronization	X	X	X
Color reconnection	X	X	X
ISR/FSR	X	X	X
PDF	X	X	X
b quark modeling	X	X	X
Muon ID and scale		X	X
Muon track		X	X
Muon isolation		X	X
Electron ID and scale	X	X	
Opposite charge	X	X	
$dZ(l, PV)$	X	X	X
Vertex Z distribution	X	X	X
Jet ID	X	X	X
Jet energy resolution	X	X	X
Jet vertex confirmation	X	X	X
Jet energy scale	X	X	X
$b-$ Jet energy scale	X	X	X
JSSR Shifting on/off	X	X	X
Z p_T reweighting	X	X	X
background cross sections	X	X	X
EM lhood fit systematics	X	X	
Background modeling	X		X
Integrated luminosity	X	X	X
Uncorrelated			
Monte Carlo statistics	X	X	X
Trigger	X	X	X
EM lhood fit statistical error	X	X	
Fake muon rate		X	X

Systematic Correlation	p17	p20
Monte Carlo statistics		
Branching fractions	X	X
Data quality	X	X
Higher order, hadronization	X	X
Color reconnection	X	X
ISR/FSR	X	X
PDF	X	X
b quark modeling	X	X
Muon ID and scale		
Muon track		
Muon isolation		
Electron ID and scale		
Opposite charge	X	X
$dZ(l, PV)$	X	X
Vertex Z distribution	X	X
Trigger		
Jet ID		
Jet energy resolution		
Jet vertex confirmation		
Jet energy scale		
$b-$ Jet energy scale	X	X
JSSR Shifting on/off	X	X
Lumi reweighting		
Z p_T reweighting	X	X
Background cross sections	X	X
Background modeling		
MET modeling		
Fake EM		
Fake muon rate		
Integrated luminosity	X	X

The combined $p\bar{p} \to t\bar{t}$ dilepton cross-section is found to be:

$$\ell\ell: \quad \sigma_{t\bar{t}} = 8.76^{+0.61}_{-0.59}\,({\rm stat})\,^{+1.00}_{-0.95}\,({\rm syst})\,^{+0.67}_{-0.60}\,({\rm lumi})\ {\rm pb}.$$

Combining this result with the published one [1] that used $1 fb^{-1}$ leads to a $t\bar{t}$ production cross sections in the dilepton channel for the top quark mass of 172.5 GeV using 5.3 fb^{-1} of:

$$\ell\ell: \quad \sigma_{t\bar{t}} = 8.44^{+0.54}_{-0.52}\,({\rm stat})\,^{+0.87}_{-0.82}\,({\rm syst})\,^{+0.67}_{-0.59}\,({\rm lumi})\ {\rm pb}. \tag{6}$$

The measured cross sections are in good agreement with the standard model prediction of $7.46^{+0.48}_{-0.67}$ pb [39].

X. SANITY PLOTS

In this section data versus simulation comparisons are presented for 3 levels of selection:

a) inclusive selection: corresponding to events selected after cut 10 without any jet requirement;

b) 2 jet selection: corresponding to events selected after cut 10 with at least two jets (see jet selection in section III);

c) full selection: corresponding to events selected after all cuts.

The $t\bar{t}$ simulation is shown normalized to the measured $t\bar{t}$ cross-section in each of the channels. For all selections the number of "fake" background is normalized to the number given by the electron likelihood fit and/or by the muon fake rate while the shape of the distribution is taken from events where the leptons have the same sign.

A. Dielectron Channel

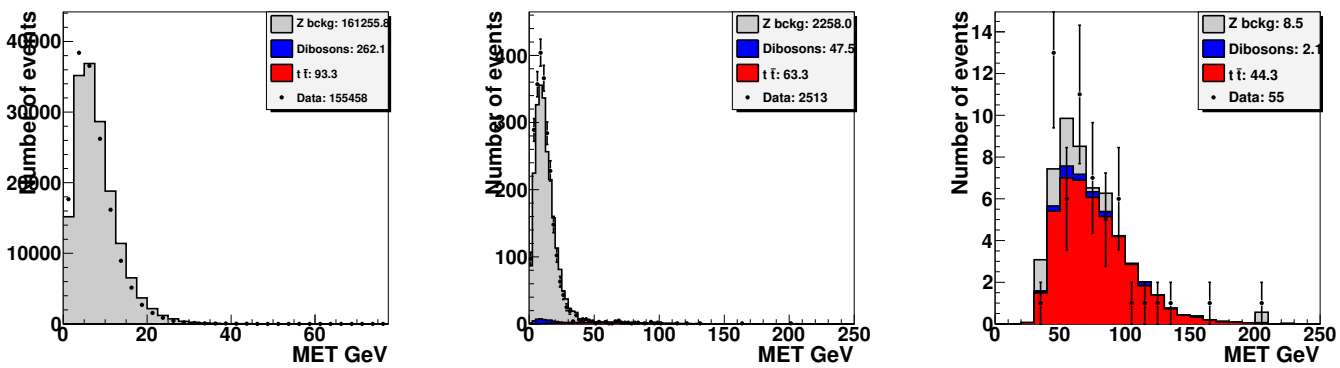

(a) Inclusive selection (b) 2 jet selection (c) Final selection.

FIG. 11: Transverse missing energy distributions in the ee channel.

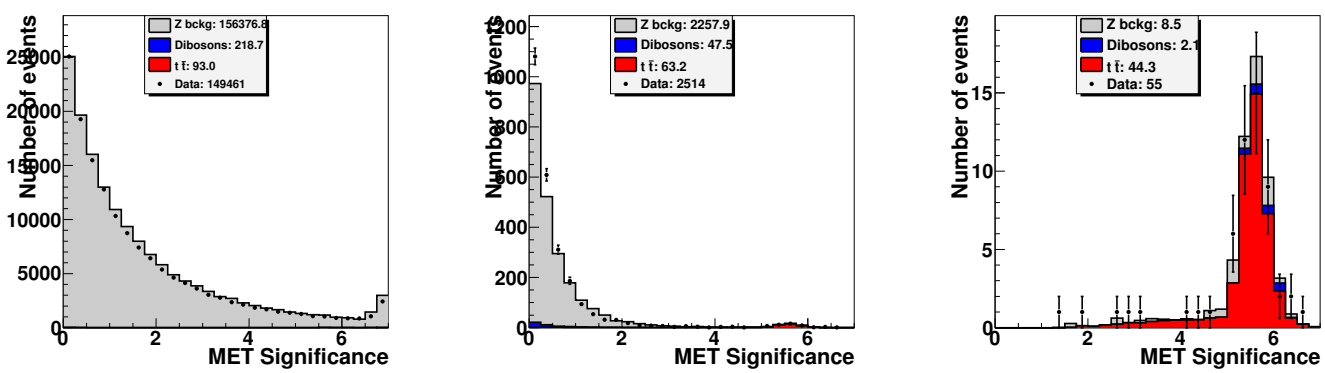

(a) Inclusive selection (b) 2 jet selection (c) Final selection.

FIG. 12: Missing energy significance in the ee channel.

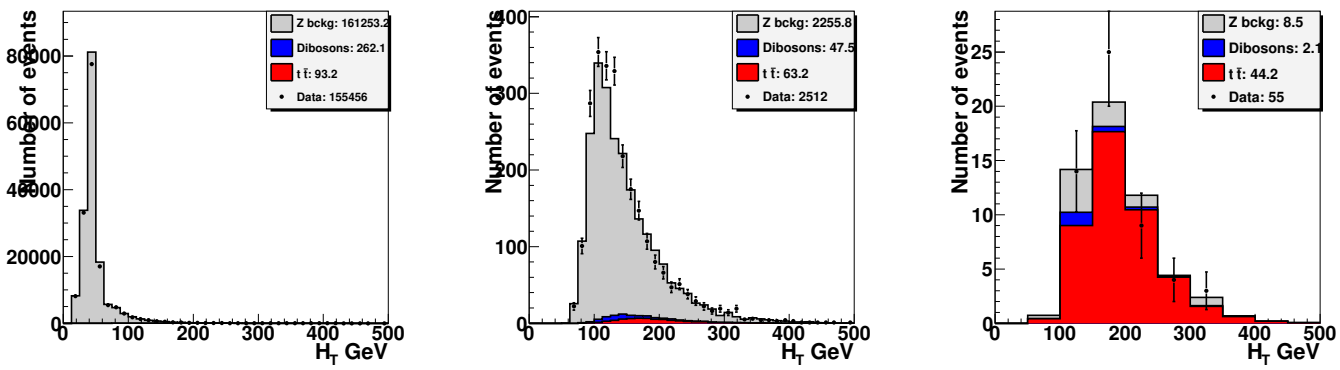

(a) Inclusive selection

(b) 2 jet selection

(c) Final selection.

FIG. 13: H_T distribution where H_T is the scalar sum of the leading lepton transverse momentum and transverse momentum of all jets in the ee channel.

(a) 2 jet selection

(b) Final selection.

FIG. 14: H: sum of the energy of the electrons and the jets in the ee channel.

(a) 2 jet selection

(b) Final selection.

FIG. 15: Aplanarity in the ee channel.

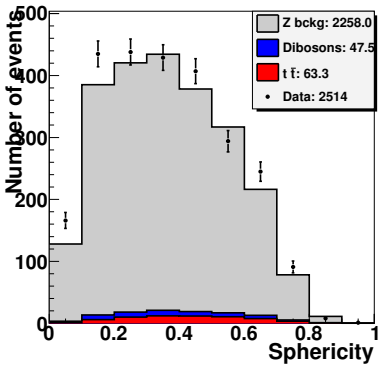

(a) 2 jet selection

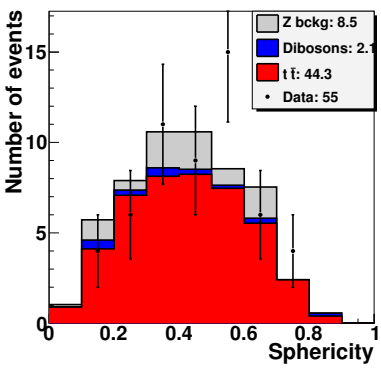

(b) Final selection.

FIG. 16: Sphericity in the ee channel.

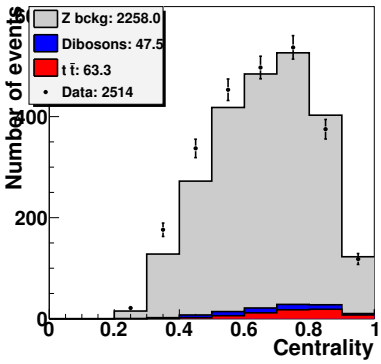

(a) 2 jet selection

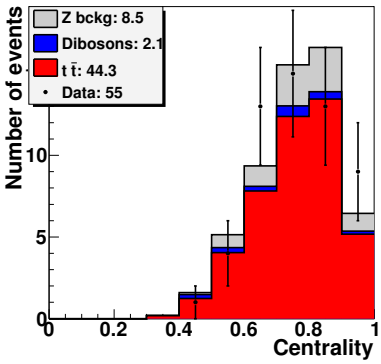

(b) Final selection.

FIG. 17: Centrality in the ee channel.

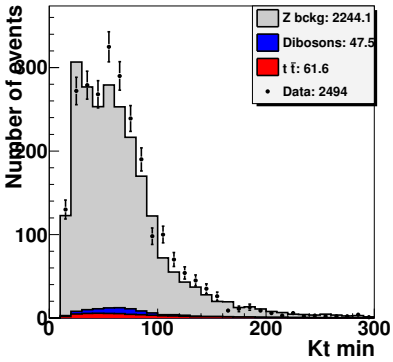

(a) 2 jet selection

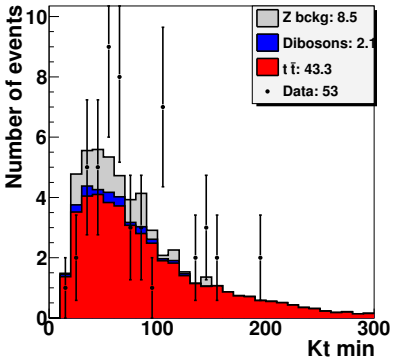

(b) Final selection.

FIG. 18: kt_{min} in the ee channel.

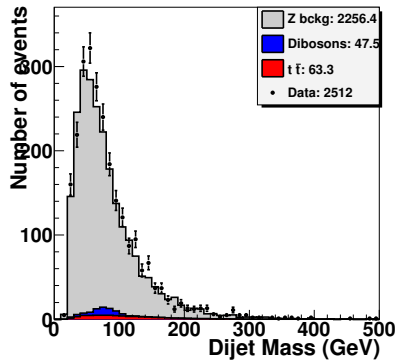

(a) 2 jet selection

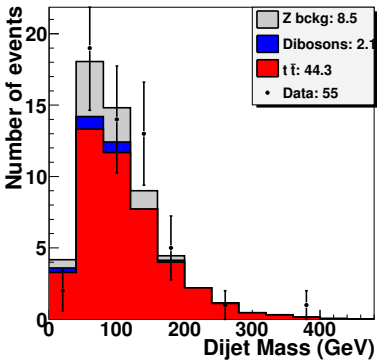

(b) Final selection.

FIG. 19: M_{jjmin} in the ee channel.

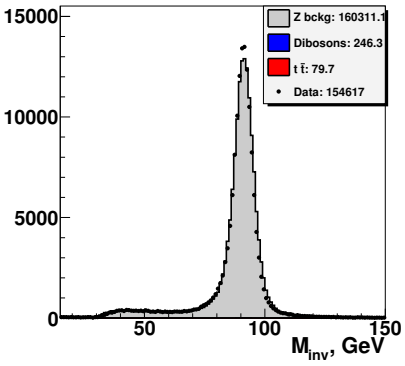

(a) Inclusive selection

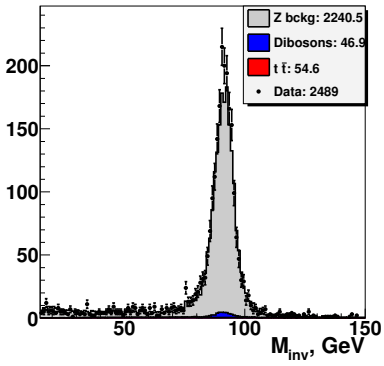

(b) 2 jet selection

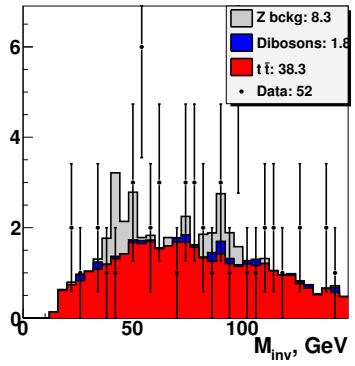

(c) Final selection.

FIG. 20: Dielectron invariant mass M_{ee} in the ee channel.

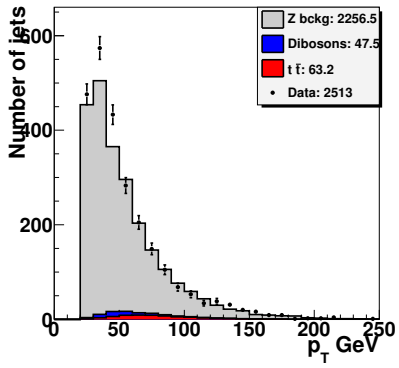

(a) 2 jet selection

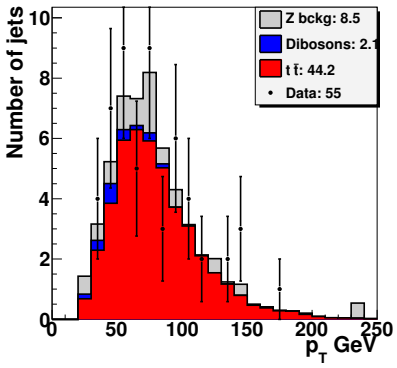

(b) Final selection

FIG. 21: Leading jet transverse momentum distribution in the ee channel.

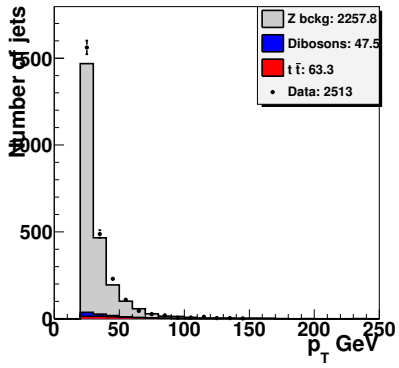

(a) 2 jet selection

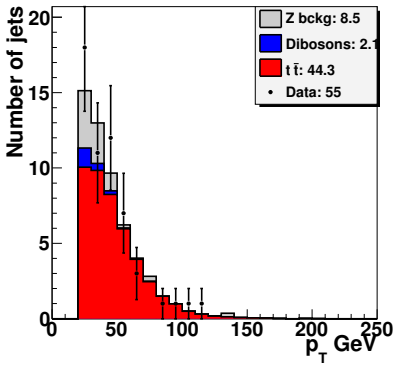

(b) Final selection

FIG. 22: Next to leading jet transverse momentum distribution in the ee channel.

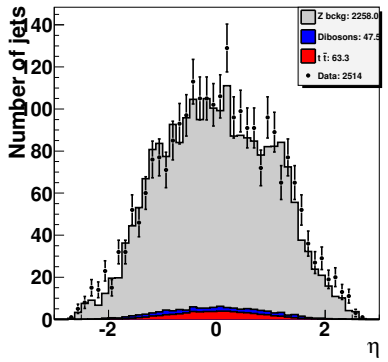

(a) 2 jet selection

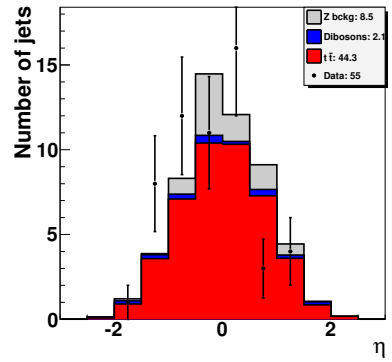

(b) Final selection

FIG. 23: Leading jet pseudo-rapidity distribution in the ee channel.

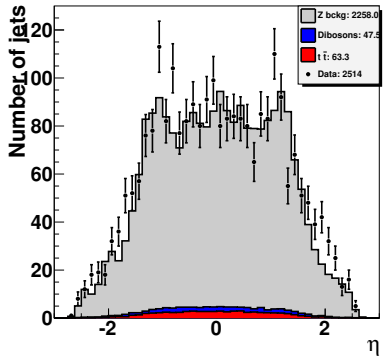

(a) 2 jet selection

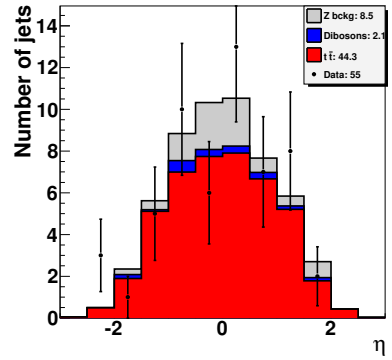

(b) Final selection

FIG. 24: Next to leading jet pseudo-rapidity distribution in the ee channel.

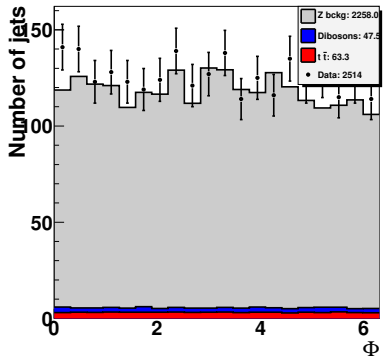

(a) 2 jet selection

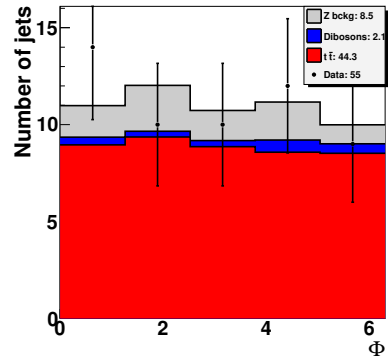

(b) Final selection

FIG. 25: Leading jet ϕ distributions in the ee channel.

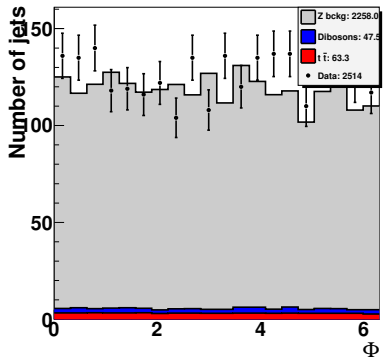

(a) 2 jet selection

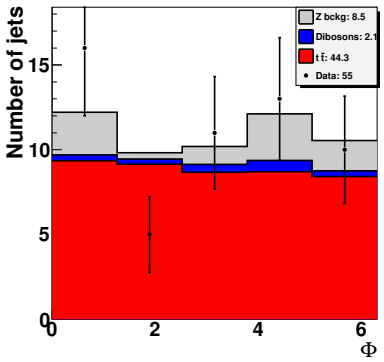

(b) Final selection

FIG. 26: Next to leading jet ϕ distributions in the ee channel.

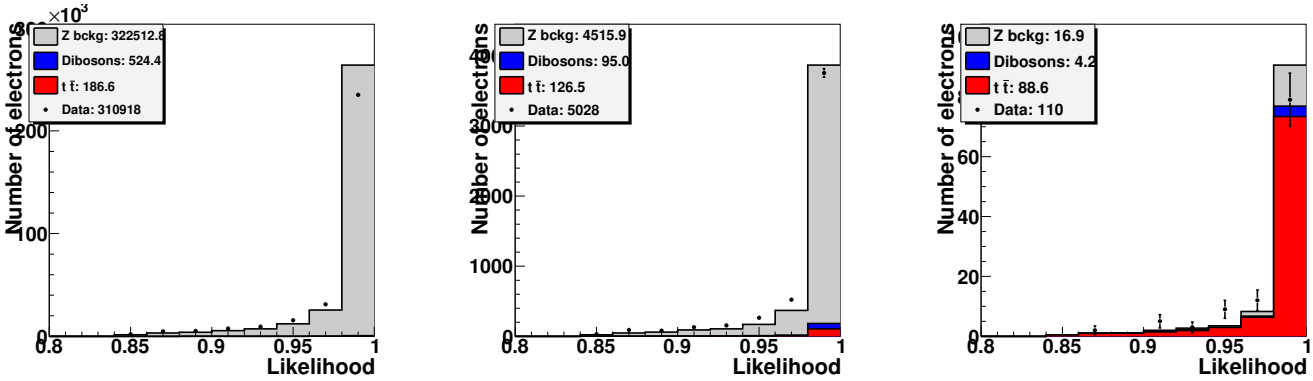

(a) Inclusive selection

(b) 2 jet selection

(c) Final selection before likelihood cut

FIG. 27: Electron likelihood distributions in the ee channel.

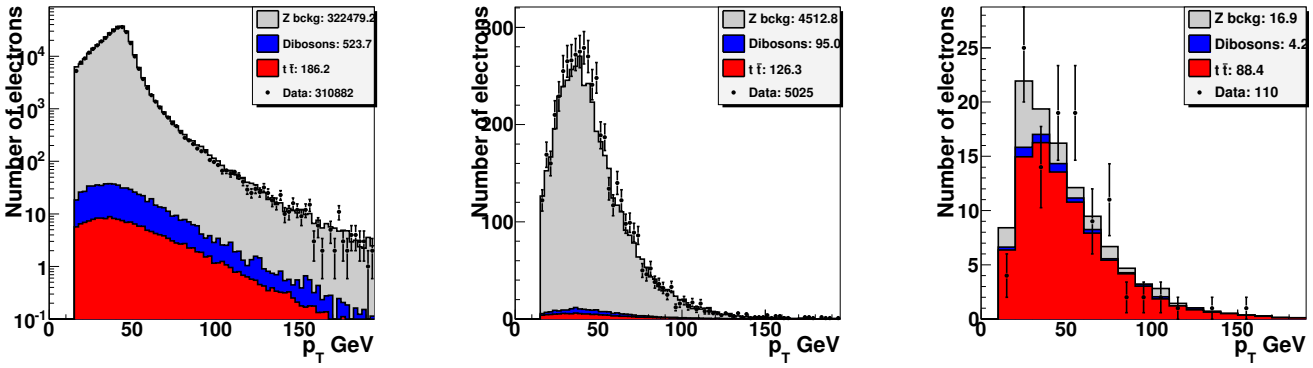

(a) Inclusive selection

(b) 2 jet selection

(c) Final selection.

FIG. 28: Electron transverse momentum distributions in the ee channel.

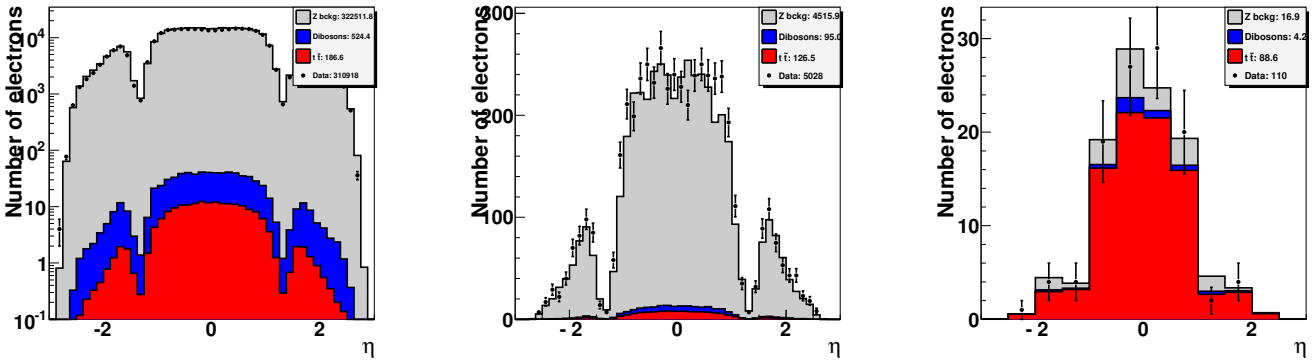

(a) Inclusive selection

(b) 2 jet selection

(c) Final selection.

FIG. 29: Electron η distributions in the ee channel.

B. Electron Muon Channel

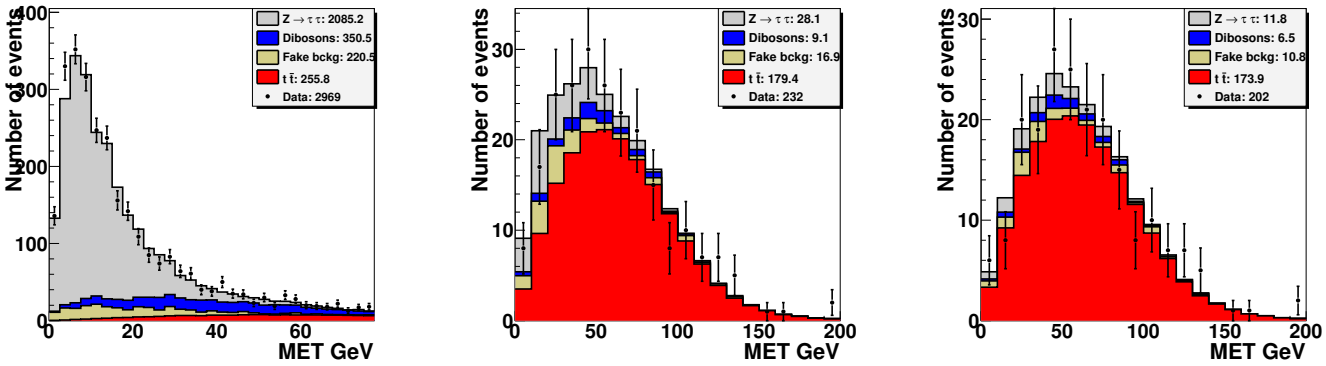

(a) Inclusive selection (b) 2 jet selection (c) Final selection.

FIG. 30: Transverse missing energy distributions in the eμ channel.

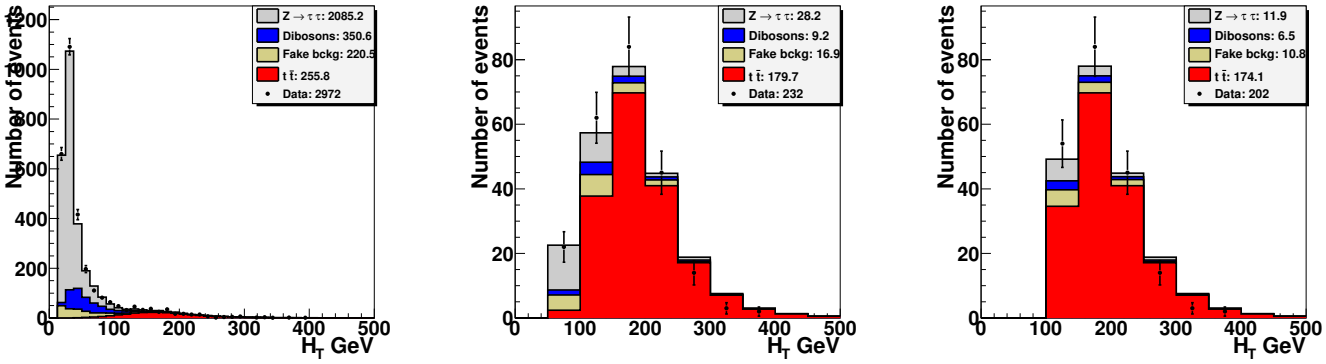

(a) Inclusive selection (b) 2 jet selection (c) Final selection.

FIG. 31: H_T distribution where H_T is the scalar sum of the leading lepton transverse momentum and transverse momentum of all jets in the eμ channel.

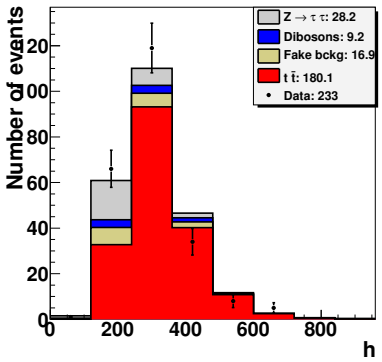

(a) 2 jet selection

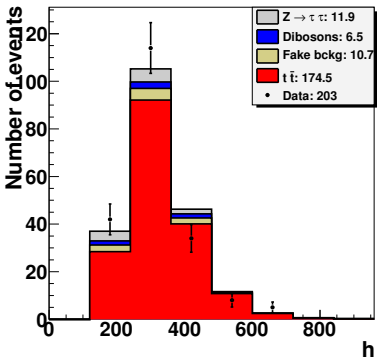

(b) Final selection.

FIG. 32: H: sum of the energy of the leptons and the jets in the eμ channel.

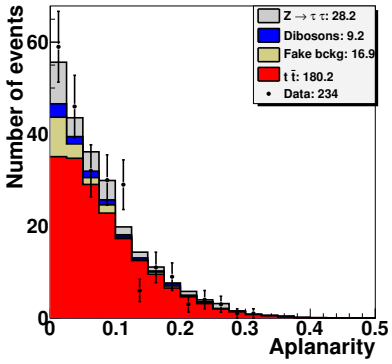

(a) 2 jet selection

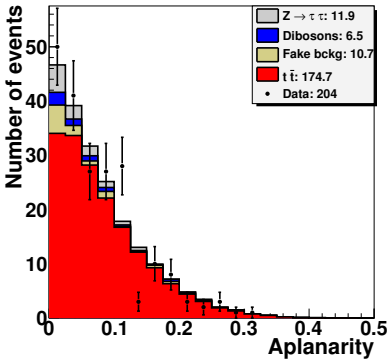

(b) Final selection.

FIG. 33: Aplanarity in the eμ channel.

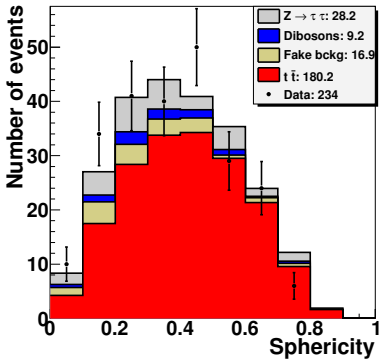

(a) 2 jet selection

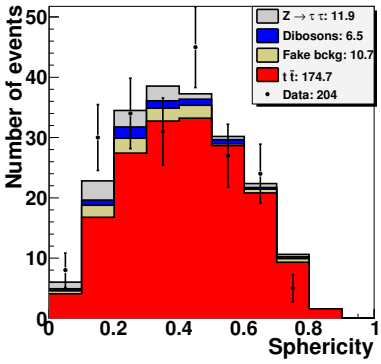

(b) Final selection.

FIG. 34: Sphericity in the eμ channel.

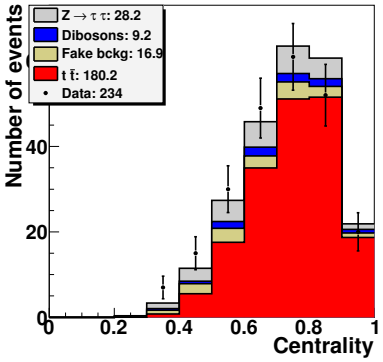

(a) 2 jet selection

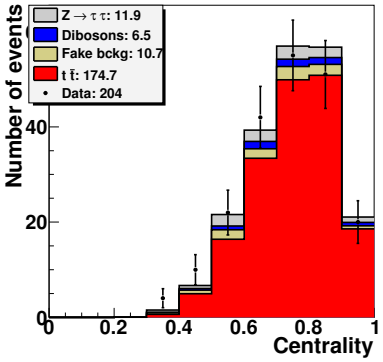

(b) Final selection.

FIG. 35: Centrality in the eμ channel.

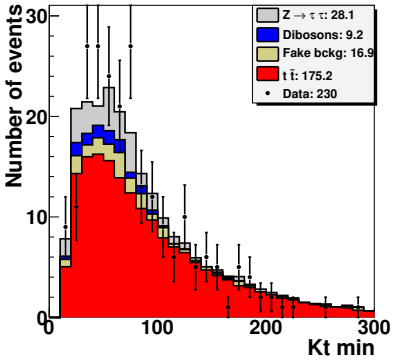

(a) 2 jet selection

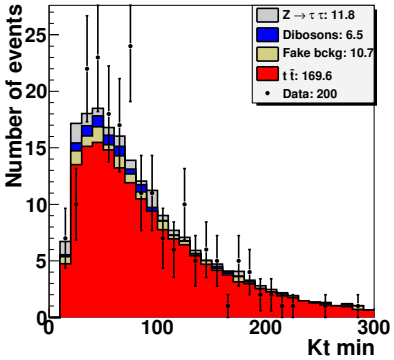

(b) Final selection.

FIG. 36: kt_{min} in the eμ channel.

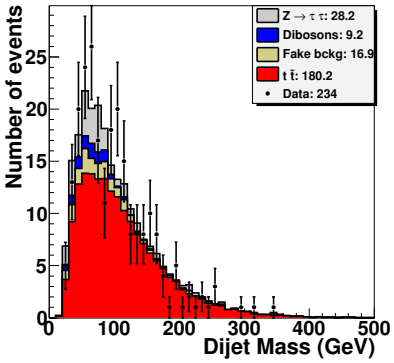

(a) 2 jet selection

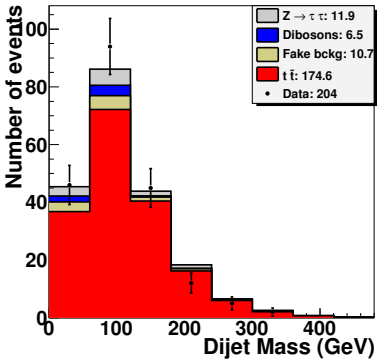

(b) Final selection.

FIG. 37: M_{jjmin} in the eμ channel.

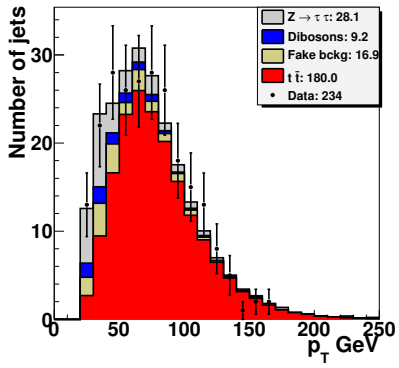

(a) 2 jet selection

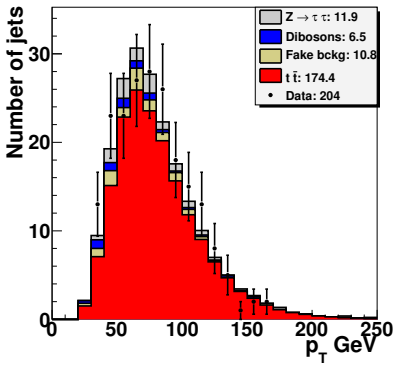

(b) Final selection

FIG. 38: Leading jet transverse momentum distribution in the eμ channel.

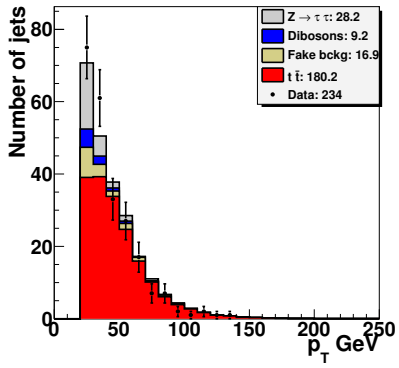

(a) 2 jet selection

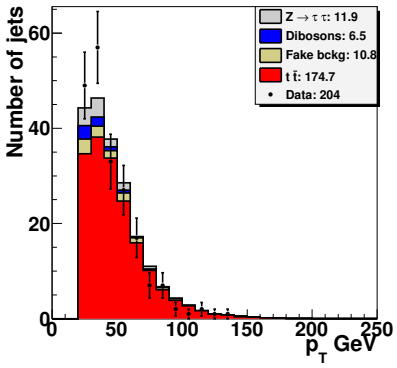

(b) Final selection

FIG. 39: Next to leading jet transverse momentum distribution in the eμ channel.

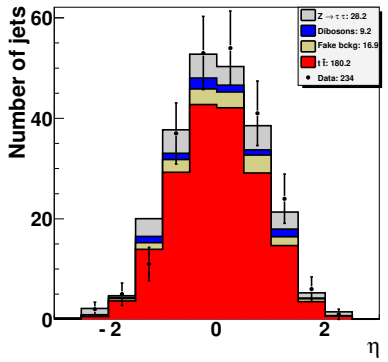

(a) 2 jet selection

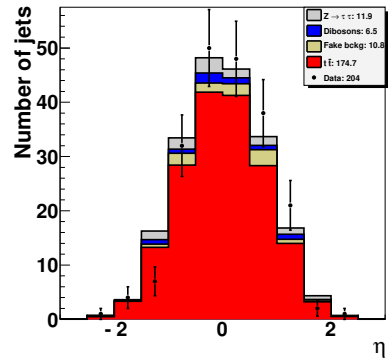

(b) Final selection. Leading jet

FIG. 40: Leading jet pseudo-rapidity distribution in the eμ channel.

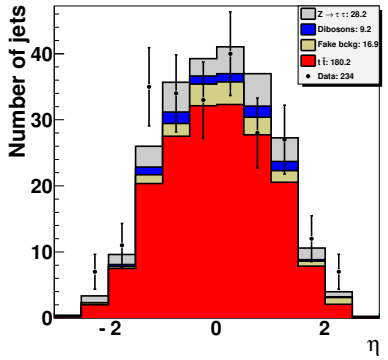

(a) 2 jet selection

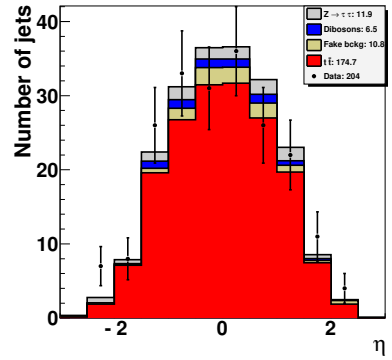

(b) Final selection

FIG. 41: Next to leading jet pseudo-rapidity distribution in the eμ channel.

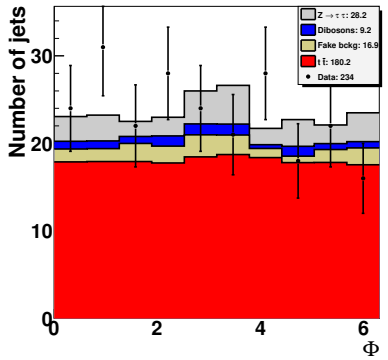

(a) 2 jet selection

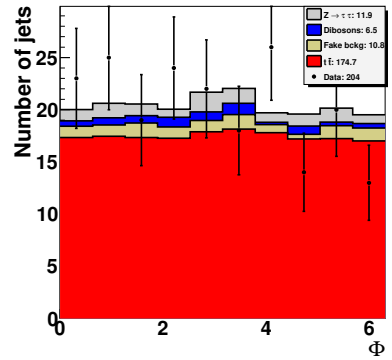

(b) Final selection

FIG. 42: Leading jet ϕ distributions in the eμ channel.

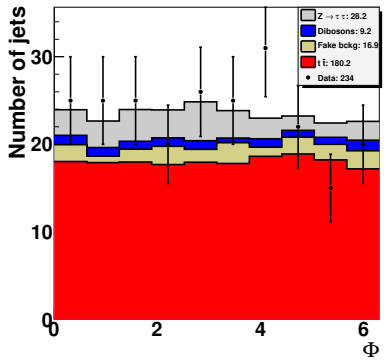

(a) 2 jet selection

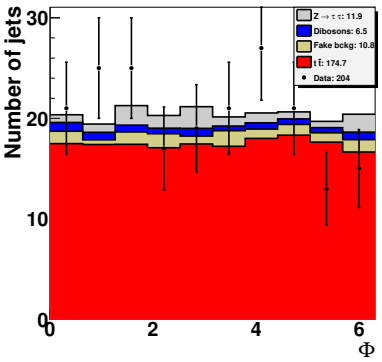

(b) Final selection

FIG. 43: Next to leading jet ϕ distributions in the eμ channel.

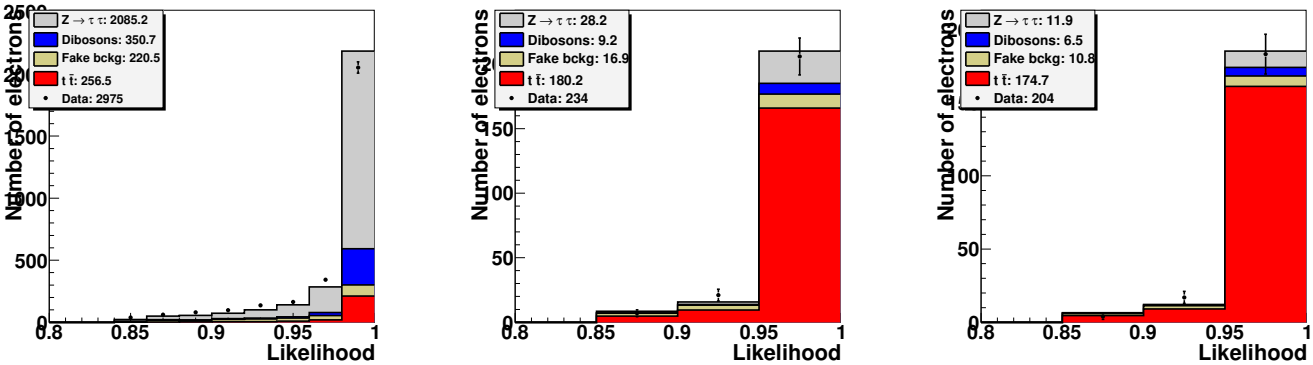

(a) Inclusive selection

(b) 2 jet selection

(c) Final selection before likelihood cut

FIG. 44: Electron likelihood distributions in the eμ channel.

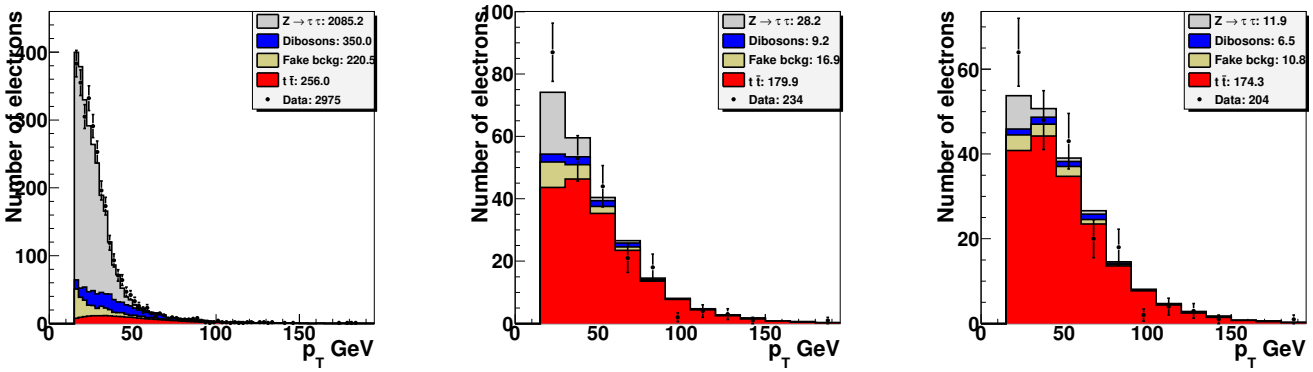

(a) Inclusive selection

(b) 2 jet selection

(c) Final selection.

FIG. 45: Electron transverse momentum distributions in the eμ channel.

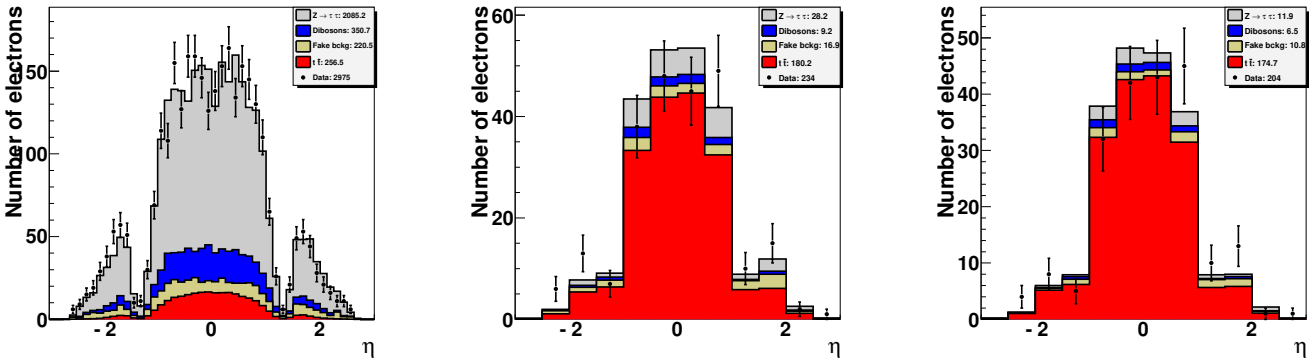

(a) Inclusive selection

(b) 2 jet selection

(c) Final selection.

FIG. 46: Electron η distributions in the eμ channel.

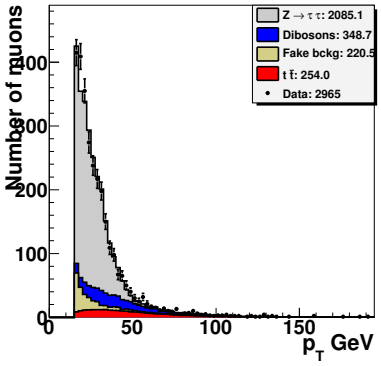

(a) Inclusive selection

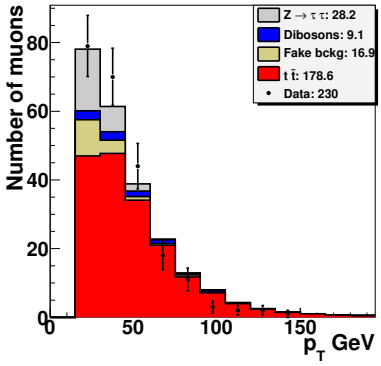

(b) 2 jet selection

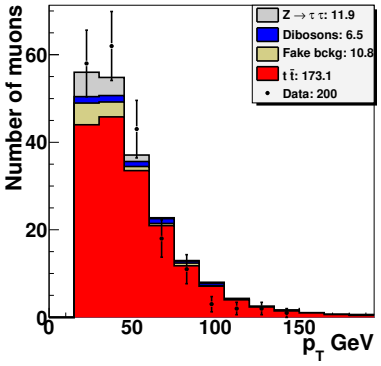

(c) Final selection.

FIG. 47: Muon transverse momentum distributions in the eμ channel.

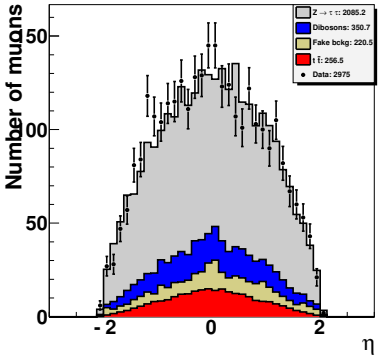

(a) Inclusive selection

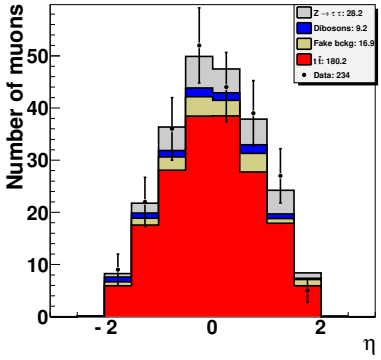

(b) 2 jet selection

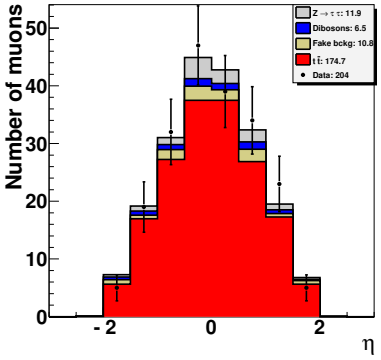

(c) Final selection.

FIG. 48: Muon η distributions in the eμ channel.

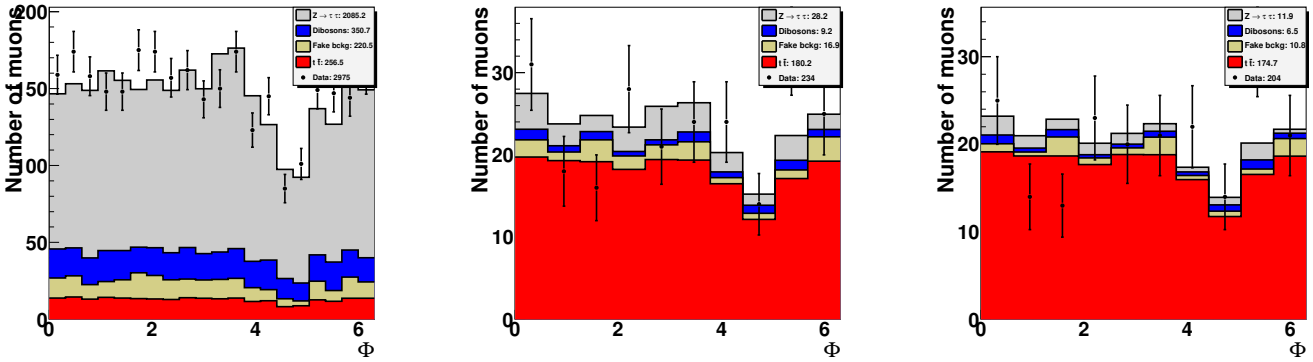

(a) Inclusive selection (b) 2 jet selection (c) Final selection.

FIG. 49: Muon ϕ distributions in the eμ channel.

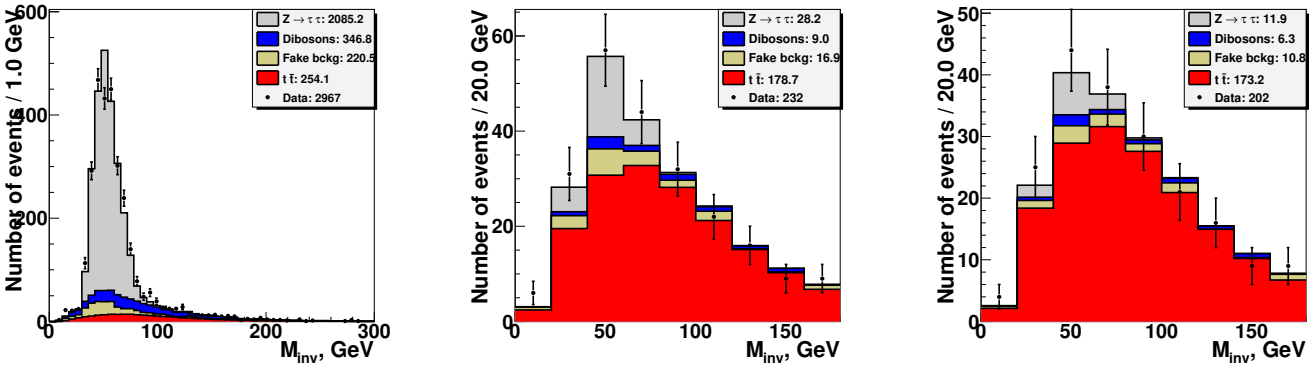

(a) Inclusive selection (b) 2 jet selection (c) Final selection.

FIG. 50: Electron - Muon Invariant Mass in the eμ channel.

C. Dimuon Channel

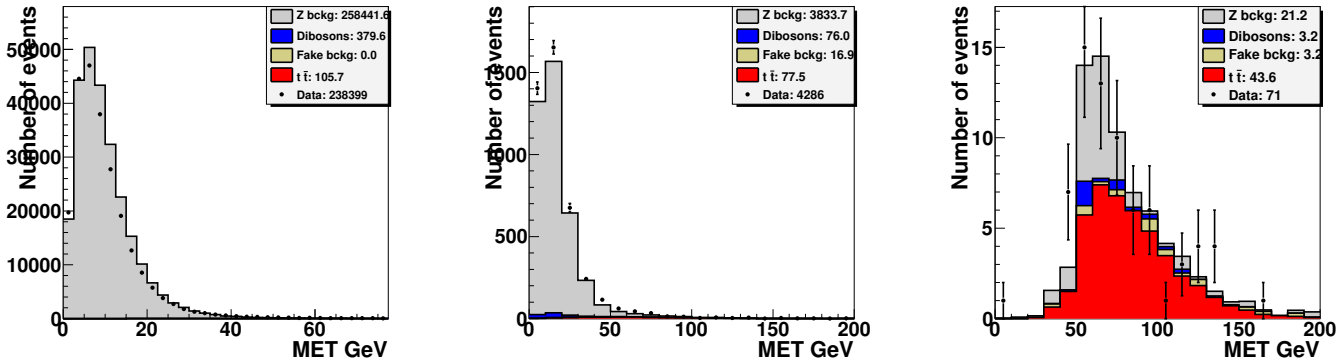

(a) Inclusive selection (b) 2 jet selection (c) Final selection.

FIG. 51: Transverse missing energy distributions in the $\mu\mu$ channel.

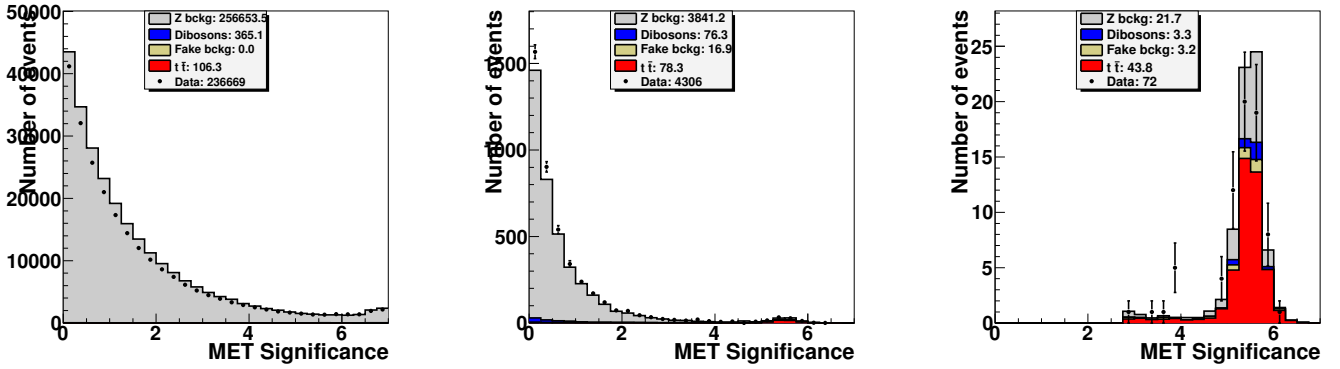

(a) Inclusive selection (b) 2 jet selection (c) Final selection.

FIG. 52: Missing energy significance in the $\mu\mu$ channel.

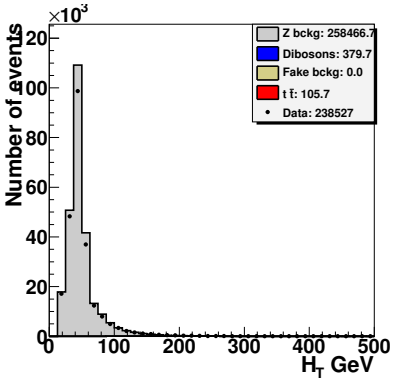

(a) Inclusive selection

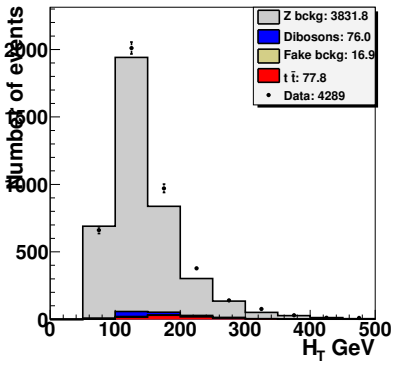

(b) 2 jet selection

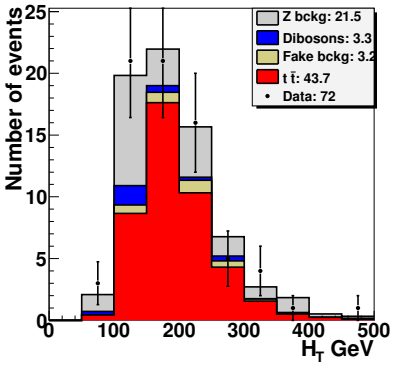

(c) Final selection.

FIG. 53: H_T distribution where H_T is the scalar sum of the leading lepton transverse momentum and transverse momentum of all jets in the $\mu\mu$ channel.

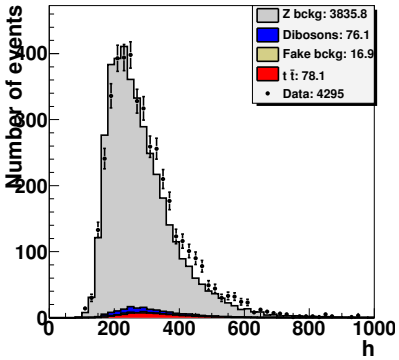

(a) 2 jet selection

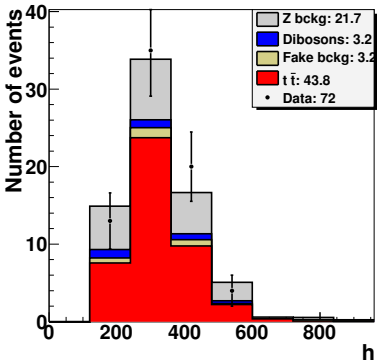

(b) Final selection.

FIG. 54: H: sum of the energy of the muons and the jets in the $\mu\mu$ channel.

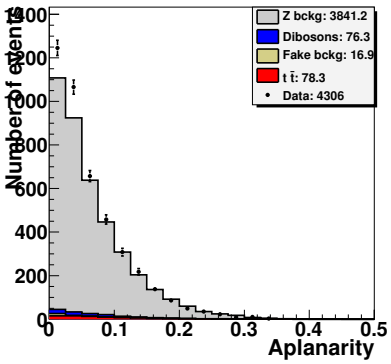

(a) 2 jet selection

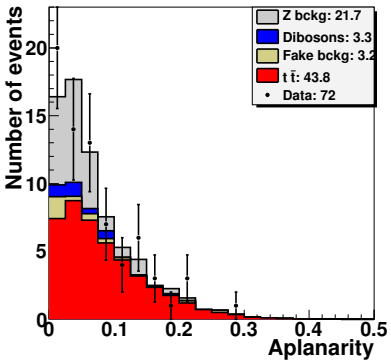

(b) Final selection.

FIG. 55: Aplanarity in the $\mu\mu$ channel.

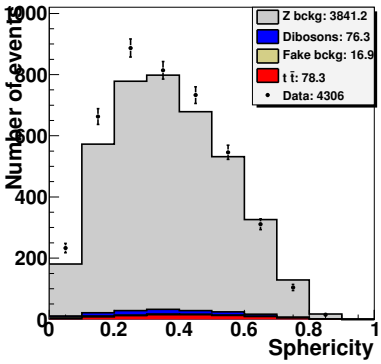

(a) 2 jet selection

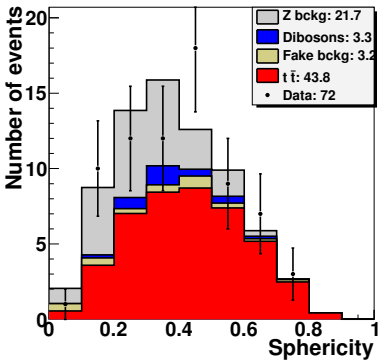

(b) Final selection.

FIG. 56: Sphericity in the $\mu\mu$ channel.

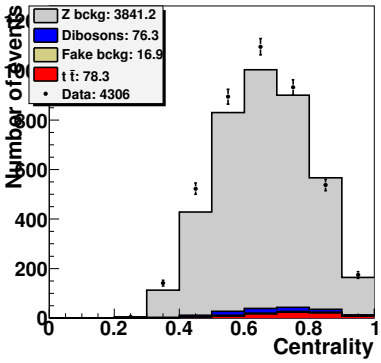

(a) 2 jet selection

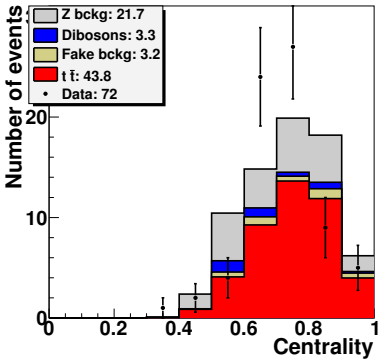

(b) Final selection.

FIG. 57: Centrality in the $\mu\mu$ channel.

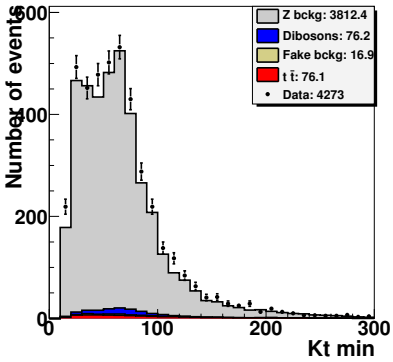

(a) 2 jet selection

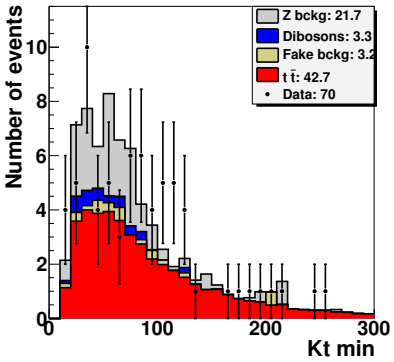

(b) Final selection.

FIG. 58: kt_{min} in the $\mu\mu$ channel.

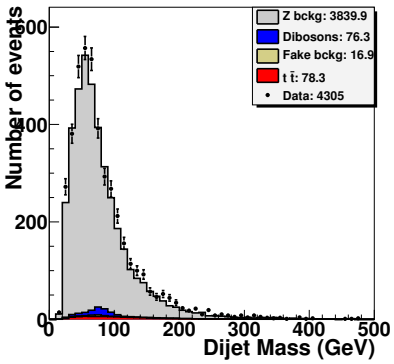

(a) 2 jet selection

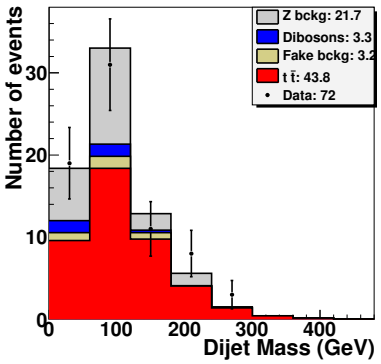

(b) Final selection.

FIG. 59: M_{jjmin} in the $\mu\mu$ channel.

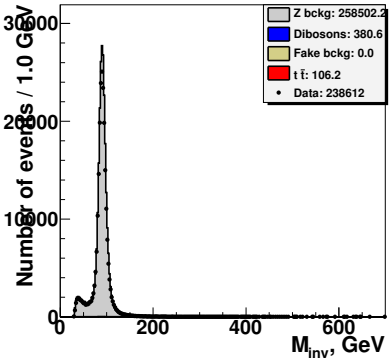

(a) Inclusive selection

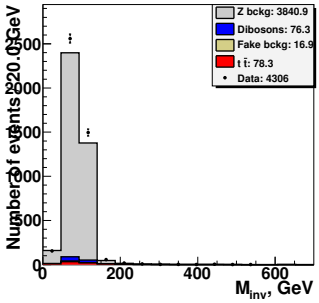

(b) 2 jet selection

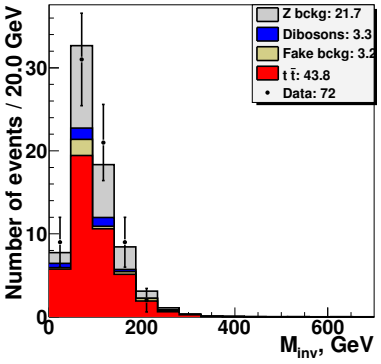

(c) Final selection.

FIG. 60: Dimuon invariant mass $M_{\mu\mu}$ in the $\mu\mu$ channel.

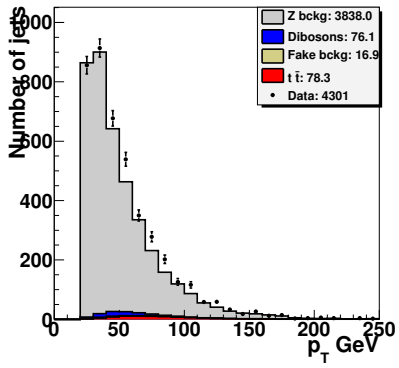

(a) 2 jet selection

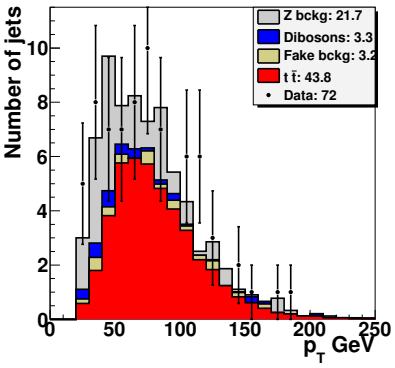

(b) Final selection

FIG. 61: Leading jet transverse momentum distribution in the $\mu\mu$ channel.

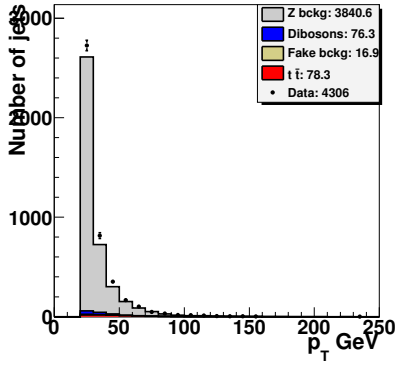

(a) 2 jet selection

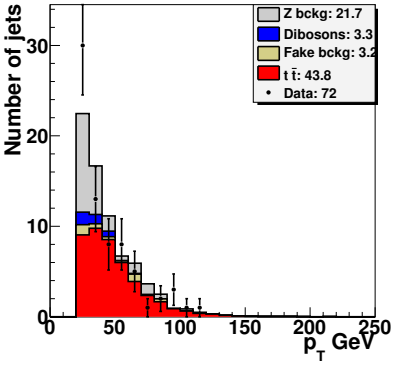

(b) Final selection

FIG. 62: Next to leading jet transverse momentum distribution in the $\mu\mu$ channel.

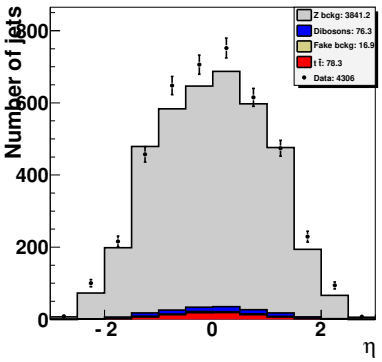

(a) 2 jet selection

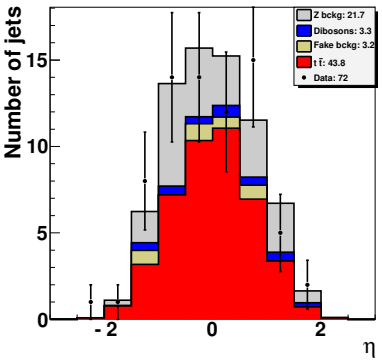

(b) Final selection

FIG. 63: Leading jet pseudo-rapidity distribution in the $\mu\mu$ channel.

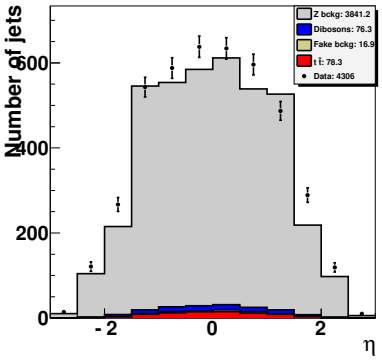

(a) 2 jet selection

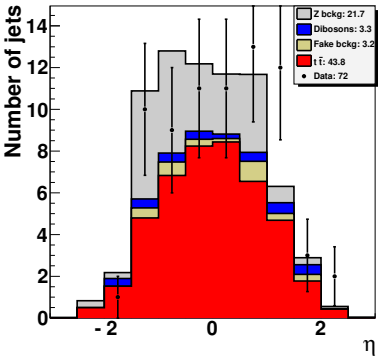

(b) Final selection

FIG. 64: Next to leading jet pseudo-rapidity distribution in the $\mu\mu$ channel.

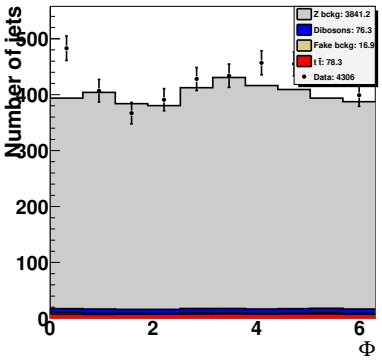

(a) 2 jet selection

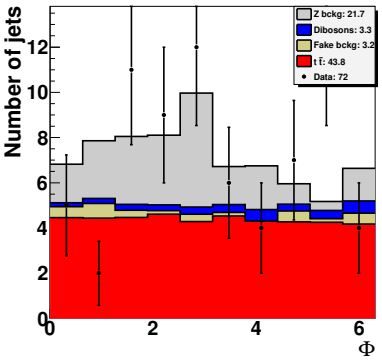

(b) Final selection

FIG. 65: Leading jet ϕ distributions in the $\mu\mu$ channel.

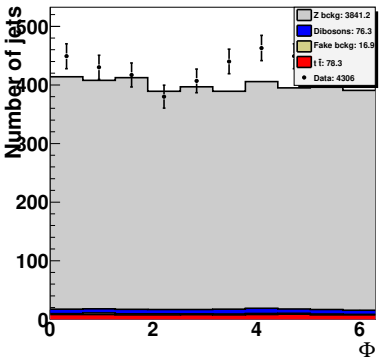

(a) 2 jet selection

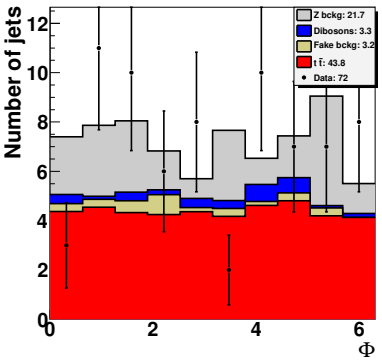

(b) Final selection

FIG. 66: Next to leading jet ϕ distributions in the $\mu\mu$ channel.

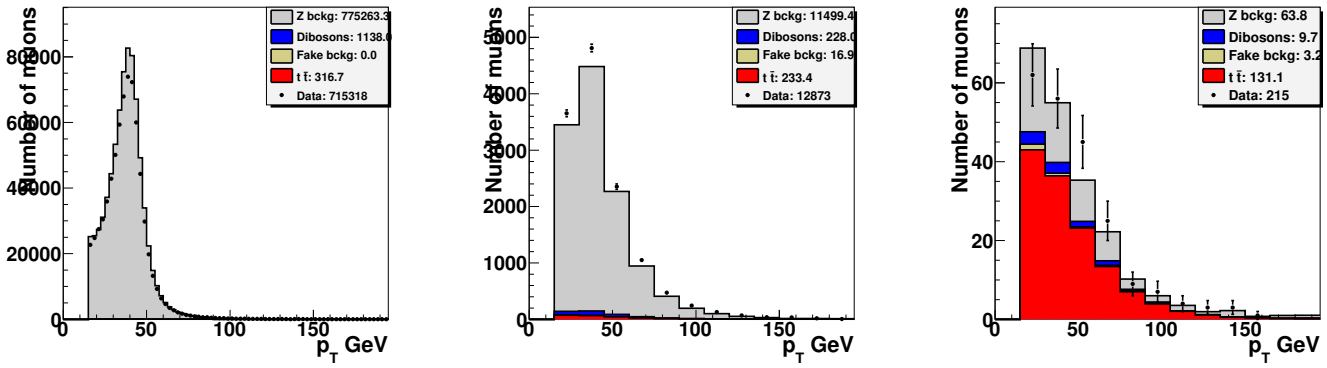

(a) Inclusive selection (b) 2 jet selection (c) Final selection.

FIG. 67: Muon transverse momentum distributions in the $\mu\mu$ channel.

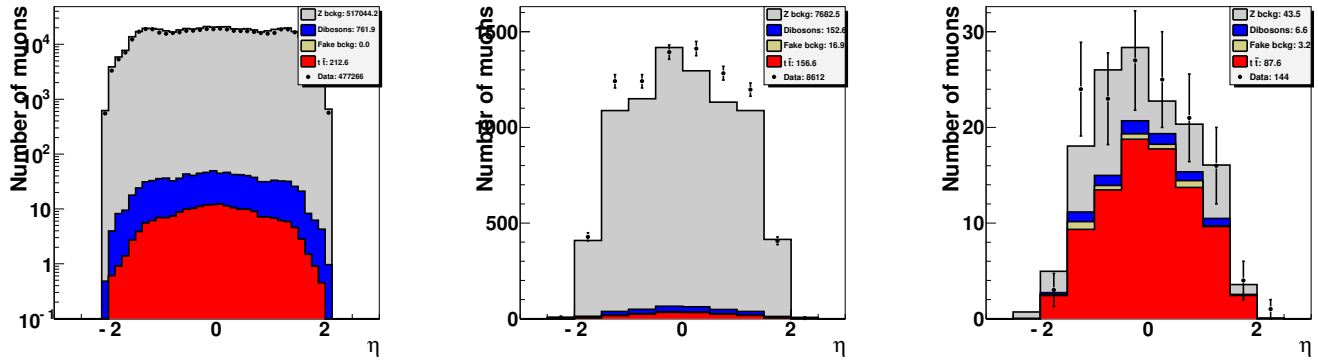

(a) Inclusive selection (b) 2 jet selection (c) Final selection.

FIG. 68: Muon η distributions in the $\mu\mu$ channel.

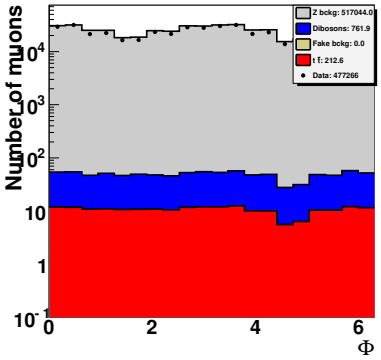

(a) Inclusive selection

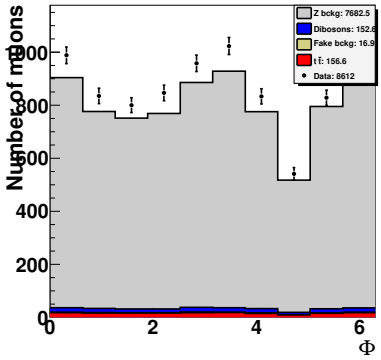

(b) 2 jet selection

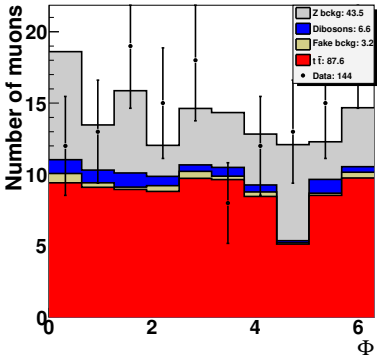

(c) Final selection.

FIG. 69: Muon ϕ distributions in the $\mu\mu$ channel.

XI. APPENDIX: TMVA INPUTS IN THE DIELECTRON CHANNEL

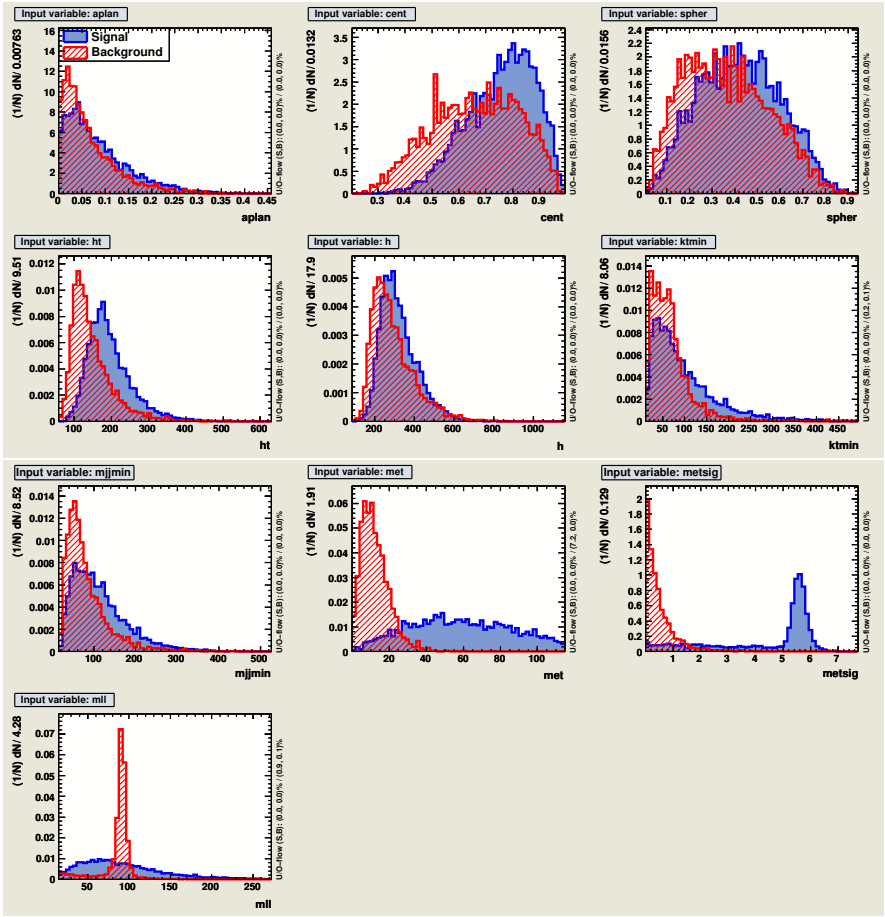

FIG. 70: Signal (red) and background (blue) separations for the input variables of the dielectron BDT.

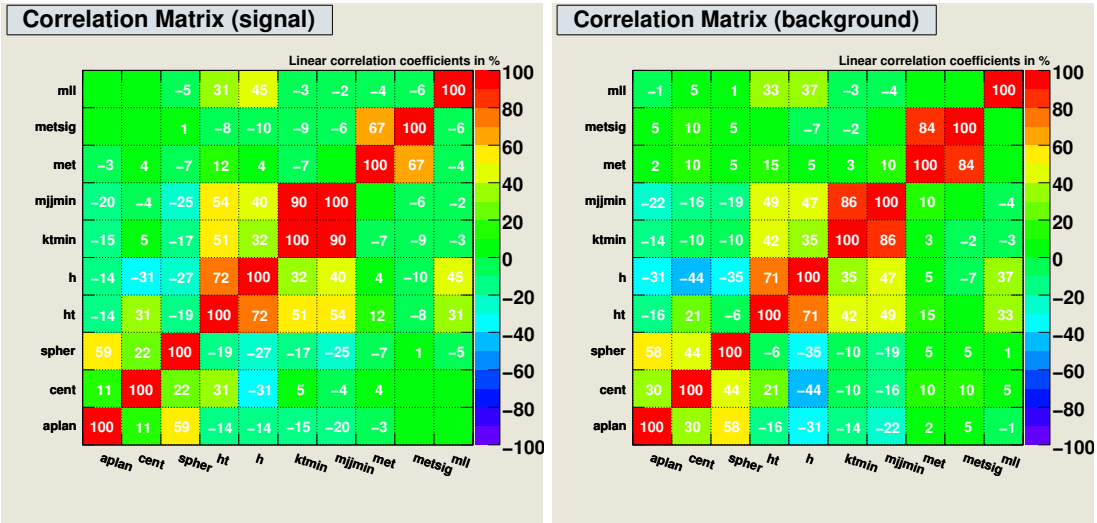

FIG. 71: Correlations between the input variables of the dielectron BDT for signal (left) and the background (right).

XII. APPENDIX: TMVA INPUTS IN THE DIMUON CHANNEL

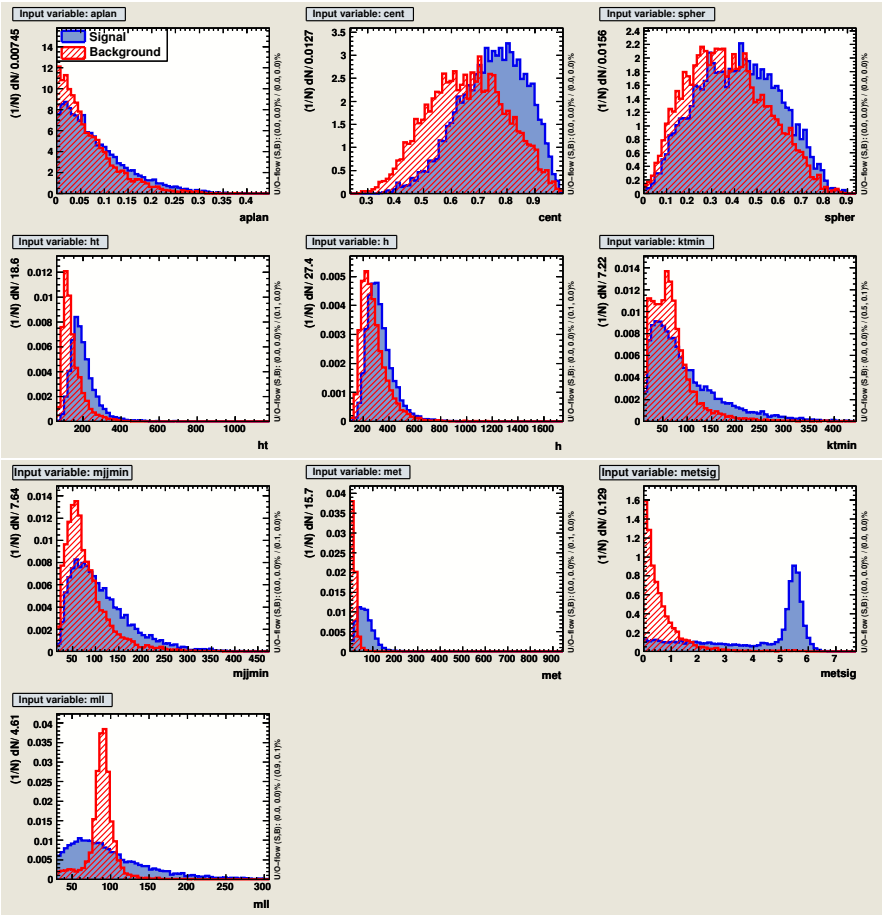

FIG. 72: Signal (red) and background (blue) separations for the input variables of the dimuon BDT.

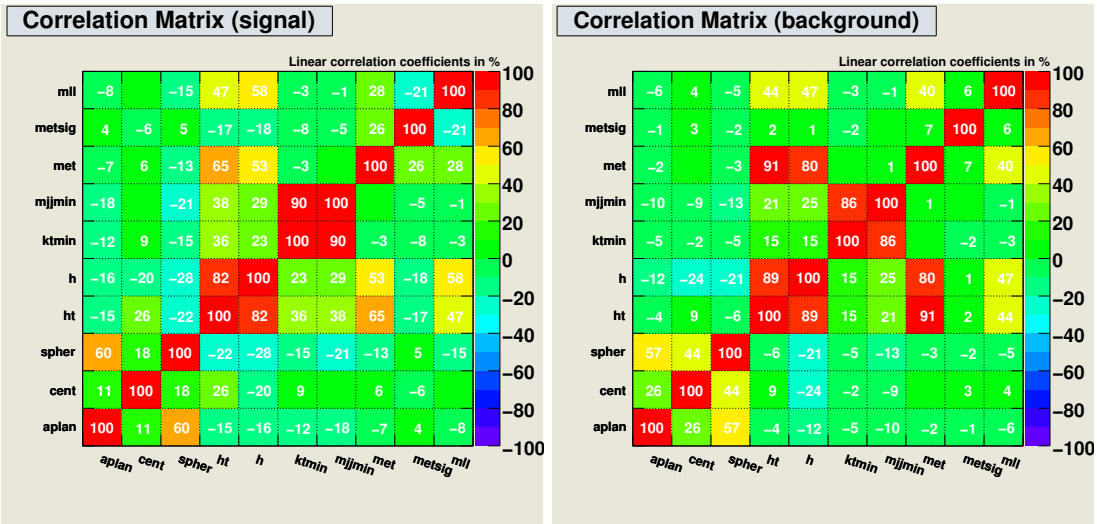

FIG. 73: Correlations between the input variables of the dimuon BDT for signal (left) and the background (right).

[1] V. M. Abazov *et al.* [D0 Collaboration], "Measurement of the ttbar production cross section and top quark mass extraction using dilepton events in ppbar collisions," Phys. Lett. B **679**, 177 (2009) [arXiv:0901.2137 [hep-ex]].

[2] M. Arthaud, M. Besançon, S. Chakrabarti, F. Déliot, E. Shabalina, V. Sharyy *Final Measurement of the ttbar Production Cross-section at sqrt(s)=1.96 TeV in Electron Muon Final States using p17 data set*, DØ Note 5580, February, 2008.

[3] B. Martin, Y. Arnoud, G. Sajot, E. Shabalina *Final Measurement of the ttbar production cross section at sqrt(s)= 1.96 TeV in the ee final state using p17 data set* DØ Note 5579, February, 2008.

[4] U. Bassler, J. P. Konrath, C. Schwanenberger, E. Shabalina *Final Measurement of the ttbar Production Cross-section at sqrt(s)=1.96 TeV in the Dimuon Final State Using p17 Data Set* DØ Note 5581, February, 2008.

[5] V. Sharyy, M. Besancon, F. Deliot *ttbar Event Selection in the Electron Muon Final State using p20 Dataset for Winter 09 Conferences* DØ Note 5864, February, 2009.

[6] M. Arthaud, M. Besancon, S. Chakrabarti, F. Deliot, V. Sharyy *ttbar Event Selection in the Electron Muon Final State using p20 Dataset*, DØ Note 5720, July, 2008.

[7] DQ web page *Infrastructure for physics analyses*, `http://www-d0.fnal.gov/computing/data_quality/d0_private/forusers.html`

[8] Laurent Duflot, *et al.*, *cal_event_quality package*, DØ Note 4614, September, 2004.

[9] F. Déliot, V. Shary, *Trigger Efficiency Measurement for the OR of Electron Muon Triggers*, DØ Note 5587, February 2008

[10] M. Owen and M. Hohlfeld, *Trigger Efficiencies for the OR of Single Electron Triggers in p17 Data*, DØ Note 5409, May, 2007

[11] Marc Hohlfeld, *Measurement of Single Electron Trigger Efficiencies for RunIIB*, DØ Note 5783, November 2008

[12] Philippe Calfayan, *ORing single muon triggers in p17 data*, DØ Note 5329, January, 2007

[13] Fabrice Couderc's talk at the summer 09 workshop:
`http://www-d0.hef.kun.nl//askArchive.php?base=agenda&categ=a09886&id=a09886s2t1/transparencies`

[14] `http://www-clued0.fnal.gov/~nunne/cross-sections/dy_cross-sections.html`

[15] C. Amsler *et al.* [Particle Data Group], Phys. Lett. B **667**, 1 (2008).

[16] J. Hays, J. Mitrevski, C. Schwanenberger, *The Program Package em_cert: Version p18-br-20*, DØ Note 5070, March 2006

[17] S.-J. Park, M. Begel, *Efficiency of the Data Quality Calorimeter Flags*, DØ Note 5324, January 2007.

[18] H. Schellman, *The longitudinal shape of the luminous region at DØ* , DØ Note 5142, June 2006.

[19] `http://tmva.sourceforge.net`

[20] A. Das and E. Varnes, *Measurement of the W Boson Helicity in Top Quark Decays Using 4 $fb1$ of RunII Data*, DØ Note 5947, June 2009.

[21] `http://hepforge.cedar.ac.uk/lhapdf`

[22] J. Hobbs, *et al.*, *Study of pp(bar) -¿ $Z/\gamma^* \rightarrow ee$ and mumu event yields as a luminosity cross check*, DØ Note 5268, October 2006.

[23] A. Schwartzman *Missing Et Significance Algorithm in RunII data*, DØ Note 4254, September 2003.

[24] J. Hays, J. Mitrevski, C. Schwanenberger, T. Toole, *ingle Electron Efficiencies in p17 Data and Monte-Carlo Using p18.05.00 d0correct*, DØ Note 5105, May 2006

[25] O. Atramentov, D. Bandurin, X. Bu, B. Calpas, E. Carrera, D. Duggan, A. Ferapontov, M. Takahashi, T. Uzbyakova, H. Yin, *Electron and Photon Identification with p20 data*, DØ Note 5761, August 2008.

[26] P. Calfayan, T. Gadfort, G. Hesketh, V. Lesne, M. Owen, R. Stroehmer, V. Sharyy, B. Tuchming, *Muon Identification Certification for p17 data*, DØ Note 5157, June 2006
O. Brandt, S.W. Cho, M. Cookc, M. Eads, D. Hedin, A. Santos, B. Tuchming, Y. Yatsunenko, S.W. Youn, *Muon Identication Certication for the Summer 2009 Extended Dataset (Run IIb-1 and -2)*, DØ Note 6025, January 2010.

[27] J. Kvita and A. Harel, *p20 Jet ID Efficiencies and Scale Factors*, DØ Note 5634, March 2008

[28] A. Harel *JetID Optimization* DØ Note 4919, September 2005.

[29] A. Harel *Capping the JES muon corrections* DØ Note 5563, January 2008.

[30] `http://www-d0.fnal.gov/phys_id/jes/d0_private/certified/certified_jes.html`

[31] Nicola Makovec and Jean-François Grivaz, *Shifting, Smearing and Removing Simulated Jets*, DØ Note 4914, November 2005
C. Ochando and J.-F. Grivaz, *SSR for p17*, DØ Note 5609, January 2008
C. Ochando, talk at the JES meeting
http://www-d0.hef.kun.nl//askArchive.php?base=agenda&categ=a08924&id=a08924s1t3/transparencies

[32] `http://www-d0.fnal.gov/phys_id/jets/jetid.html`

[33] J. Kozminski *et al.*, *The electron likelihood in p14*, DØ Note 4449, November 2003
A. Kumar, B. Choudhary, J. Kozminski, R. Kehoe, J. Hays, J. Stark, *Electron Likelihood Study*, DØ Note 4769, March 2005
L. Wang, J. Hays, J. Mitrevski, C. Schwanenberger *Electron Likelihood Efficiency in p17*, DØ Note 5114, May 2006.

[34] `http://www.thep.lu.se/~torbjorn/Pythia.html`
see also T. Sjöstrand, L. Lönnblad, S. Mrenna and P. Skands, hep-ph/0308153;
and T. Sjöstrand, P. Edén, C. Friberg, L. Lönnblad, G. Miu, S. Mrenna and E. Norrbin, Comp. Phys. Commun. **135** (2001) 238, hep-ph/0010017.

[35] J. Campbell and R.K. Ellis, MCFM - Monte Carlo for FeMtobarn processes, `http://mcfm.fnal.gov/`

[36] V.Sharyy, *How to reweight MC according to the luminosity profile in data*, https://plone4.fnal.gov/P1/D0Wiki/comp/caf/caffaq/LumiReWeight

[37] M.L. Mangano, M. Moretti, F. Piccinini, R. Pittau, A. Polosa, ALPGEN, a generator for hard multiparton processes in hadronic collisions, JHEP **0307** (2003) 1, hep-ph/0206293; `http://mlm.home.cern.ch/mlm/alpgen/`

[38] R. J. Barlow, Nucl. Instrum. Meth. A **297**, 496 (1990).

[39] S. Moch and P. Uwer, JHEP 09, 127 (2008)
S. Moch and P. Uwer, Phys. Rev. D **78** (2008) 034003 [arXiv:0804.1476 [hep-ph]].

[40] T. Adams, *et al*, *Combination of the top quark pair production cross section, cross section ratios and top quark mass extraction*, DØ Note 5854, February 2009

[41] , T. Adams, *et al*, *Combination of the top quark pair production cross sections and search for charged Higgs boson*, DØ Note 5597, February 2008

[42] P. Sinervo, in *Proceedings of Statistical methods in Particle Physics, Astrophysics, and Cosmology*, edited by L. Lyons, R.P. Mount and R. Reitmeyer (SLAC, Standford, 2003), p 334.

[43] D. Bandurin and M. Takakhashi, *Electron charge misidentification for p17 and p20 data and Monte Carlo*, DØ Note 5927, May 2009.

[44] J. Pumplin, D.R. Stump, J.Huston, H.L. Lai, P. Nadolsky, W.K. Tung *New Generation of Parton Distributions with Uncertainties from Global QCD Analysis*, JHEP O207 (2002) 012, February, 2002.

[45] Y. Peters, M. Begel, K. Hamacher and D. Wicke, *Reweighting of the fragmentation function for the D0 Monte Carlo*, DØ Note 5325, January 2007.

[46] A. Harel, *Data over MC, b over light jet response corrections for RunIIa JES*, DØ Note 5654, April 2008.

[47] `https://plone4.fnal.gov/P1/D0Wiki/object-id/emid/emcert/Moriond2009/uncertainty_moriond09`

[48] EMid conveners, private communication.

[49] M. Arthaud, F. Deliot, B. Tuchming, V. Sharyy, D. Vilanova, *Muon Momentum Oversmearing for p20 Data*, DØ Note 5449 July 2007.

[50] T. Andeen et al., FERMILAB-TM-2365 (2007)

[51] F. Déliot, C. Schwanenberger, E. Shabalina, M. Wang, D. Wicke and Z. Ye, *Systematic Uncertainties in Top Quark Measurements*, DØ Note 6024, January 2010.

[52] M. Cacciari et al., JHEP **09** (2008) 127

[53] N. Kidonakis, R. Vogt, Phys. Rev. D **78** (2008) 074005.